Adaptive Directional Stratification for controlled estimation of the probability of a rare event

M. Munoz Zuniga[a,b], J. Garnier[a], E. Remy[b], E. de Rocquigny[c]

[a]*Laboratoire de probabilités et modèles aléatoires, Université Paris VII, Case courrier 7012, 2 place Jussieu, 75251 Paris cedex 05, France*
[b]*EDF R&D, 6 quai Watier, 78400 Chatou, France*
[c]*Ecole Centrale Paris, Grande Voie des Vignes, 92295 Chatenay-Malabry, France*

Abstract

Within the structural reliability context, the aim of this paper is to present a new accelerated Monte-Carlo simulation method, named ADS - Adaptive Directional Stratification -, and designed to overcome the following industrial constraints: robustness of the estimation of a low structural failure probability (less than 10^{-3}), limited computational resources and complex (albeit often monotonic) physical model. This new stochastic technique is an original variant of adaptive accelerated simulation method, combining stratified sampling and directional simulation and including two steps in the adaptation stage (ADS-2). First, we theoretically study the properties of two possible failure probability estimators and get the asymptotic and non-asymptotic expressions of their variances. Then, we propose some improvements for our new method. To begin with, we focus on the root-finding algorithm required for the directional approach: we present a stop criterion for the dichotomic method and a strategy to reduce the required number of calls to the costly physical model under monotonic hypothesis. Lastly, to overcome the limit involved by the increase of the input dimension, we introduce the ADS-2^+ method which has the same ground as the ADS-2 method, but additionally uses a statistical test to detect the most significant inputs and carries out the stratification only along them. To conclude, we test the ADS-2 and ADS-2^+ methods on academic examples in order to compare them with the classical structural reliability methods and to make a numerical sensitivity analysis over some parameters. We also apply the methods to a flood model and a nuclear reactor pressurized vessel model, to practically demonstrate their interest on real industrial examples.

Key words: Reliability, Failure probability, Sampling, Directional, Stratification

1. Introduction

1.1. Industrial context

Structural reliability is a domain of long-standing interest in the context of industrial safety and reliability that motivated the development of dedicated algorithms, notably for the efficient computation of low probabilities of occurrence of threshold-exceedance or failure events, such as FORM-SORM, directional sampling and importance sampling ([1, 2, 3]). The present research is inspired by the continuing difficulties encountered in some key industrial applications when tackling the issue of controlling the robustness of existing algorithms. Two different models are taken for inspiration and benchmark: a flood model and a nuclear reactor pressurized vessel

fracture mechanics model. Although it is a simplified one, the flood model is studied because it remains physically realistic and is sufficiently simple to be a test model on which a large number of structural reliability methods can be applied. The nuclear reactor pressurized vessel model is the core one that motivated this work: the mathematical and numerical constraints inherent to this model constituted our framework.

Flood

The purpose is to estimate the risk of a flood to run over a dyke, which is generally equivalent to model the "maximum highness flow of the flood" by hydraulic equations. The modelling depends on various physical parameters, the exact number depending on the sophistication of the chosen model. We denote by H the water height, this one being calculated by maximizing the water height during the flood event. The flood event is itself calculated by solving a partial differential equation system (typically from Navier-Stokes equations). A simplified analytic model can give an approximation of H. We denote by Q the watercourse flow, L the watercourse section length studied, B the watercourse width, K_s the watercourse bed friction coefficient or Strickler coefficient, Z_m and Z_v respectively the upstream and the downstream bottom watercourse height above the sea level, H_d the dyke height and Z_b the bank height. The water height simplified model takes into account all these variables:

$$H = \left(\frac{Q}{K_s B \sqrt{\frac{Z_m - Z_v}{L}}} \right)^{3/5} . \tag{1}$$

The model is usually expressed in overflow height: $S = Z_c - Z_d$ with $Z_c = (Z_v + H)$ and $Z_d = H_d + Z_b$. Among the model inputs, there are many uncertainties, like intrinsic phenomenon randomness or lack of knowledge. Here, we make the choice that the following variables are known precisely: $L = 5000$ (m), $B = 300$ (m), $Z_b = 55.5$ (m), $H_d = 0$ (m) and the next ones are considered as random: Q, K_s, Z_m, Z_v. Table 1.1 presents the distributions taken by the random physical variables (see Appendix A for an explanation of the meaning of the parameters), supposedly uncorrelated. For more details on this model we refer to [4].

Random var.	Distribution	Parameters
Q ($\mathrm{m}^3\mathrm{s}^{-1}$)	Gumbel	$a = 1013$, $b = 558$
K_s ($\mathrm{m}^{1/3}\mathrm{s}^{-1}$)	Gaussian	$\mu = 30$, $\sigma = 7.5$
Z_v (ASL m)	Triangular	$(a+b+c)/3 = 50$, $b - c = c - a = 1$
Z_m (ASL m)	Triangular	$(a+b+c)/3 = 55$, $b - c = c - a = 1$

Table 1.1 Distributions of the random physical variables of the flood model.

Note that a Gumbel distribution is a classical extreme value description for the watercourse flow. A Gaussian distribution for the friction coefficient K_s represents the metrological errors that embody most of the associated uncertainties. For the bottom watercourse heights, Z_v and Z_m, triangular distributions illustrate a geomorphological variability limited to well-known bounds yet more likely to return to its mean equilibrium value than a uniform distribution.

Nuclear reactor pressure vessel

During the normal operation of a nuclear power plant, the nuclear reactor pressure vessel (NRPV) walls are exposed to neutron radiation, resulting in localized embrittlement of the vessel steel and

weld materials in the area of the reactor core. If an embrittled NRPV has an existing manufacturing flaw of critical size and if severe system transients occur, the flaw might propagate very rapidly through the vessel, resulting in a through-wall crack and challenging the integrity of the NRPV. The severe transients of concern, known as pressurized thermal shock, are characterized by a rapid cooling (i.e. thermal shock) of the internal NRPV surface and downcomer, which may be followed by repressurization of the NRPV. Thus, a pressurized thermal shock event poses a potentially significant challenge to the structural integrity of the NRPV. For more details, we refer to [5].

The NRPV fast fracture thermo-mechanical model during an accidental situation includes three parts. Firstly, a simplified thermo-hydraulic representation of the accidental event, which analytically describes, as functions of the time and the security injection temperature, T_{si}, the primary fluid temperature, the pression and the heat transfer coefficient between primary coolant and vessel cladding. Secondly, a thermo-mechanical model of the vessel cladding thickness, incorporating the vessel material properties depending on the temperature. Lastly, a rupture model around a manufacturing flaw, including different variables: (a) a variable, h, representing the dimension of an axial type flaw, underclad and located in the base metal, (b) a stress intensity factor with plastic correction, (c) the toughness depending on the temperature at the flaw and the RT_{NDT}, whose discrepancy with the fluence is evaluated with some codified forecasting formulas called FIM ([6]).
In practice, the modelling of the NRPV may assign probabilistic distributions to some physical sources of uncertainty. In this article, a maximum of 7 input physical variables will be considered as random. The next table summarizes the distributions of the independent physical random inputs of the NRPV model (see Appendix A for an explanation of the meaning of the parameters).

Random var.	Distribution	Parameters
h (mm)	Weibull	$a = 0.02, b = 3.09, c = 1.80$
ΔRT_{NDT} ($^\circ$ C)	Gaussian	$\mu = FIM, \sigma = 8.1$
K_{Ic} (MPa m$^{0.5}$)	Uniform	$a = 0, b = 100$
Ratio height/length	Lognormal	$a = 0.02, ln(b) = -1.53, ln(c) = 0.55$
Azimut flaw ($^\circ$ C)	Uniform	$a = 0, b = 360$
Thickness sheathing (mm)	Uniform	$a = 7.5, b = 9$
T_{si} ($^\circ$ C)	Uniform	$a = 9, b = 35$

Table 1.2 Distributions of the random physical variables of the NRPV model.

The failure event is defined as follows: at least at one time t during the accidental situation, the instantaneous failure function, G, becomes negative. So, we are looking for an evaluation of the following probability: $P_f = \mathbb{P}\big(G_{Min}(\mathbf{X}) < 0\big)$ with $\mathbf{X}$ the random input vector and $G_{Min}(\mathbf{X}) = \min_t(G(\mathbf{X}, t))$. The practical difficulty for the evaluation of this probability comes from the fact that it involves high computational times: indeed, each calculation of $G_{Min}(\mathbf{x})$ for a fixed value of the input vector requires the evaluation of $\big(G(\mathbf{x}, t)\big)_t$ for fixed random value of each variable, and then a minimization along the duration of the simulated accidental situation, which can be sizeable in CPU time.
Another point to be mentioned is that the failure function G is monotonic with respect to some variables, as in many industrial mechanical models and structural reliability applications where inputs are mostly either of a resistance-type (hence increasing margin) or a load-type (hence decreasing margin) [4]. Notice that the results of this paper must be considered as textbook ex-

ercises, which can not be used to draw conclusions about the integrity or safety assessment of nuclear power plants.

1.2. Mathematical modelling for failure probability problems

One way to assess the reliability of a structure from physical considerations is to use a probabilistic approach: it includes the joint probability distribution of the random input variables of the deterministic model representing the physical behaviour of the studied structure. We consider a real-valued failure function, $G : \mathbb{D} \subset \mathbb{R}^p \to \mathbb{R}$, which typically represents a failure margin predicted by a numerical deterministic model. A probability space $(\mathbb{D}, \mathcal{A}, \mathbb{P})$ is defined in order to model the uncertainties, giving to $\mathbf{X}$, the input variable vector, the nature of a random vector. Then, we assume that the probability density function f of the random vector $\mathbf{X}$ exists and is known.
In this context, we want to assess the failure probability P_f:

$$P_f = \mathbb{P}(G(\mathbf{X}) < 0) = \int_{G(\mathbf{x})<0} f(\mathbf{x})d\mathbf{x} \tag{2}$$

with G the failure function defined over $\mathbb{D}$, $\mathbf{X} = (X^1, ..., X^p)$ the p-dimensional random vector of the input variables and f the density function of $\mathbf{X}$. We partition the set where G is defined, $\mathbb{D}$, into three subsets: the reliability domain, denoted by $\mathbb{D}_r := \{\mathbf{x} \in \mathbb{D}, G(\mathbf{x}) > 0\}$, the failure domain, denoted by $\mathbb{D}_f := \{\mathbf{x} \in \mathbb{D}, G(\mathbf{x}) < 0\}$, and the boundary between the two previous subsets, the limit state surface, denoted by $\mathbb{D}_l := \{\mathbf{x} \in \mathbb{D}, G(\mathbf{x}) = 0\}$. Furthermore, four key features characterize our agenda:

- G may be complex and greedy in computational resources: even when involving high performance computing, industrial constraints limit typically to a maximum of a few thousands evaluations of G,
- no continuity or derivability assumptions are considered for G.
- the failure is a rare event, which means that P_f is very small. In this work, we will consider that a small probability is a probability lower than 10^{-3}.
- the results must be robust, i.e. with explicit and trustworthy error control. In fact, these results might be presented to the NSA (Nuclear Safety Authority) in some decision process (maintenance inspection program, decision lifetime extension...) and, consequently, must come with guarantees.

The first two constraints correspond to our hypotheses and the last constraint is the key goal motivating this research. Remember in fact that larger failure probabilities are mostly satisfactorily treated by classical alternatives e.g. crude Monte-Carlo sampling; conversely, efficient heuristics do exist for smaller failure probabilities although error control remains partial if not inexistent (e.g. FORM/SORM) as detailed hereafter.

1.3. Analysis of the existing strategies

Many stochastic tools already exist in the literature to estimate a failure probability. A well-developed state of the art can be found in [7, 8, 9] with a large bibliography. From a global point of view, the numerical integration methods are not effective when the dimension p of $\mathbb{D}$ is large.

Methods such as sparse grid are currently under development to overcome the curse of dimensionality. However, these methods require smoothness assumptions to be efficient [10, 11, 12]. Consequently, these optimized numerical integration methods, potentially efficient, are inadequate in our context. Another standard solution consists in keeping the real physical model coupled with the FORM/SORM numerical approximation [13, 1]. However, in non-analytic cases, the error carried out is not easily calculable, even if the calculation times remain reasonable [13]. The last solution is to evaluate the integral (2) by Monte-Carlo simulation [7, 14]. This method is reliable and controllable thanks to probabilistic theorems, which give an accurate statistical measure of the estimation error. Nevertheless, the required number of simulations is unrealistic for a rare failure problem and a complex physical model. There exist accelerated methods which reduce the variance of the failure probability estimator [15, 7, 16, 17, 18, 19]. But the estimation error control is only asymptotic and, consequently, only valuable for a sufficient number of simulations. All of them may be combined with a response surface approach, replacing the initial physical model by a simplified one with numerical approximation. This last alternative includes for instance the largely-developing non-intrusive chaos polynomial approaches. Besides, coupling any of those with a response surface approach generally adds another source of error, which enjoys only very limited error control. In this article, we choose to reflect over the simulation methods rather than the response surface methods. Within the context of structural reliability applications, the Monte-Carlo sampling basis remains therefore generally the reference. This state of fact brings us to consider the accelerated Monte-Carlo methods and try to develop a new one, which "converges" as fast as possible and enables to obtain an estimation error control in a reasonable number of simulations.

2. The ADS method

We turn our attention to the stratified sampling and the directional simulation methods. On the one hand, the stratified sampling offers the opportunity to carry out an adaptive strategy and the possibility to take advantage of a potential monotonic hypothesis of the model G: [7, 15, 20, 21]. On the other hand, the use of the directional sampling method enables to keep a good "precision/calculation time" ratio: [1, 22, 23]. That is why we decided to combine these two methods and their advantages to develop our new stochastic technique. Thus, the aim of this article is to present and concretely demonstrate the interest of a new accelerated simulation method, we named ADS - Adaptive Directional Stratification -, and which we designed to overcome the real industrial constraints listed above.
Our purpose here is to estimate the following expectation:

$$I = \mathbb{E}\big(F(\mathbf{X})\big) \tag{3}$$

by a new accelerated Monte-Carlo simulation method, for some bounded measurable function F. The stratification method is widely used for the estimation of expectations in various contexts such as survey, finance, reliability... The directional simulation method is essentially used in structural reliability for failure probability estimations, but here we present it in the general case of an expectation estimation. We just keep in mind that for all our failure probability estimation applications, the function F is of the form: $F(\mathbf{x}) = \mathbb{1}_{G(\mathbf{x})<0}$ which has all the required properties.

2.1. Preliminary: stratification, directional sampling and optimization

The idea is to take advantage of the possibilities given by the stratification and directional simulation methods: optimal allocation result, adaptive strategy, efficient small probability estimation, reasonable calculation time.
I can be expressed as follows: $I = \mathbb{E}\big(\xi(\mathbf{A})\big)$ with

$$\xi(\mathbf{a}) = \mathbb{E}\big(H(R\mathbf{A})|\mathbf{A} = \mathbf{a}\big) = \int H(r\mathbf{a}) f_R(r) dr, \tag{4}$$

where f_R is the density function of R, $H = F \circ T_{Nataf}^{-1}$ and T_{Nataf}^{-1} the inverse Nataf transformation, such that $\mathbf{U} = F \circ T_{Nataf}^{-1}(\mathbf{X})$ is a Gaussian random vector. $\mathbf{U}$ can be expressed as $\mathbf{U} = R\mathbf{A}$ with R^2 a chi-square random variable, $\mathbf{A}$ a random vector uniformly distributed over the unit sphere $S_p \subset \mathbb{R}^p$ and R independent with $\mathbf{A}$ [24]. At this point, we introduce the

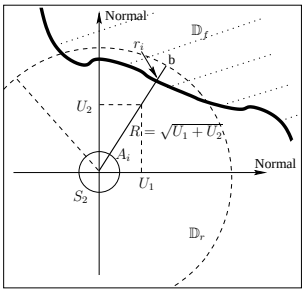

Fig. 2.1 Two dimensional illustration of the directional simulation method in the Gaussian space.

stratification method by partitioning the "directional space", in other words the space where $\mathbf{A}$ takes its values, that is to say the p-dimensional unit sphere S_p. The natural strata adapted to directional draws are cones and partitioning S_p is equivalent to make a partition of the general space into cones. Let us denote by $(q_i)_{i=1,\dots,m}$ a partition of S_p into m strata.
Let us denote by n the total number of directional draws and consider an allocation of directional draws in each stratum described by the sequence $w = (w_i)_{i=1,\dots,m}$ such that $\sum_{i=1}^m w_i = 1$. The number of draws in the i-th stratum is $n_i = \lfloor n w_i \rfloor$ with $\lfloor . \rfloor$ the floor function.
We can express the expectation $I = \mathbb{E}\big(\xi(\mathbf{A})\big)$ as:

$$I = \sum_{i=1}^{m} \mathbb{P}(\mathbf{A} \in q_i) \mathbb{E}\big(\xi(\mathbf{A}^i)\big) = \sum_{i=1}^{m} \rho_i I_i \tag{5}$$

with $\mathbf{A}^i \sim \mathcal{L}(\mathbf{A}|\mathbf{A} \in q_i)$ uniformly distributed over q_i and $I_i = \mathbb{E}\big(\xi(\mathbf{A}^i)\big)$.
Now, we estimate I_i by drawing n_i directions in the i-th stratum. This can be done by using a simple rejection method. We get:

$$\hat{I}_i = \frac{1}{n_i} \sum_{j=1}^{n_i} \xi(\mathbf{A}_j^i) \tag{6}$$

with $(\mathbf{A}_j^i)_{j=1,\dots,n_i}$ a family of independent and identically distributed random variables with the distribution $\mathcal{L}(\mathbf{A}|\mathbf{A} \in q_i)$.

We obtain the following unbiased estimator by coupling the directional sampling and the stratification methods:

$$\hat{I}^{DSS} = \sum_{i=1}^{m} \rho_i \hat{I}_i \tag{7}$$

and its variance is given by σ^2_{DSS}/n with

$$\sigma^2_{DSS} = \sum_{i=1}^{m} \frac{\rho_i^2 \sigma_i^2}{w_i} \tag{8}$$

where $\sigma_i^2 = Var\big(\xi(\mathbf{A}^i)\big)$.
Then, we get the following asymptotical result:

$$\sqrt{n}(\hat{I}^{DSS} - I) \xrightarrow[n\to+\infty]{\mathcal{L}} \mathcal{N}(0, \sigma^2_{DSS}). \tag{9}$$

Now, just like in the standard stratification method, we can determine the optimal allocation of directional draws in each stratum in order to minimize the variance estimator given by (8), which can be useful for the design of an adaptive strategy. The unique solution of this constraint optimization problem is given by the sequence defined by:

$$w_i^{opt_1} = \frac{\rho_i \sigma_i}{\sum_{j=1}^{m} \rho_j \sigma_j} \tag{10}$$

for $i = 1, ..., m$. The optimal variance obtained with this allocation is: $\sigma^2_{opt_1}/n$ with

$$\sigma^2_{opt_1} := \left(\sum_{i=1}^{m} \rho_i \sigma_i \right)^2. \tag{11}$$

Now, we can see that the variance of the estimator $\hat{I}^{DSS}$ with the optimal allocation is smaller than the one with the proportional one. Besides, we demonstrate that the variance of $\hat{I}^{DSS}$ with the proportional allocation, and a fortiori with the optimal one, is: (a) smaller than the variance of the usual stratified estimator (in the Gaussian space) with a proportional or an optimal allocation, (b) smaller than the variance of the standard directional simulation method. All these variances are also smaller than the one of the standard Monte-Carlo.
Before presenting the adaptive strategy, we can imagine that we have to draw directions in a stratum where we have already drawn some directions. Let us split the total number of simulations n into two parts $\gamma_1(n)n$ and $\gamma_2(n)n$ such as $\gamma_1(n) + \gamma_2(n) = 1$. Let us assume that we have already drawn a sizeable deterministic proportion, β_i, of $\gamma_1(n)n$ in the i-th stratum and that now we want to draw a proportion w_i of $\gamma_2(n)n$ in this stratum. At the end, we will have drawn $\gamma_1(n)\beta_i n + \gamma_2(n) w_i n$ in the i-th stratum, for all i. Of course, $\sum_{i=1}^m \beta_i = 1$ and $\sum_{i=1}^m w_i = 1$. Then, the variance of the estimator will be:

$$\frac{1}{n} \sum_{i=1}^{m} \frac{\rho_i^2 \sigma_i^2}{\gamma_1(n)\beta_i + \gamma_2(n) w_i}. \tag{12}$$

Now, we can try to calculate the $(w_i)_{i=1,...,m}$ which will minimize variance (12). The associated constraint optimization problem has a unique solution, which can be computed by the following

algorithm.

Algorithm 1 :

(a) Compute, for $i = 1, ..., m$, the quantities $\frac{\beta_i}{\rho_i \sigma_i}$ and sort them in decreasing order, denoting them $\frac{\beta_{(i)}}{\rho_{(i)}\sigma_{(i)}}$. Compute, for $i = 1, ..., m$, the quantities:

$$\frac{1 + \frac{\gamma_1(n)}{\gamma_2(n)} \sum_{j=i+1}^{m} \beta_{(j)}}{\frac{\gamma_1(n)}{\gamma_2(n)} \sum_{j=i+1}^{m} \rho_{(j)}\sigma_{(j)}}.$$

(b) Denote i^* the largest i such that

$$\frac{\beta_{(i)}}{\rho_{(i)}\sigma_{(i)}} \geq \frac{1 + \frac{\gamma_1(n)}{\gamma_2(n)} \sum_{j=i+1}^{m} \beta_{(j)}}{\frac{\gamma_1(n)}{\gamma_2(n)} \sum_{j=i+1}^{m} \rho_{(j)}\sigma_{(j)}}.$$

If this inequality is false for all i, then, by convention, set $i^* = 0$.

Let us denote by $K \subset \{1, ..., m\}$ the subset defined by:

$$K = \left\{ i \in \{1, ..., m\}, (i) \leq i^* \right\} \tag{13}$$

where i^* is defined in algorithm 1. Its complementary is denoted by K^c. Thus, the unique solution of the previous optimization problem is the sequence defined by:

$$w_i^{opt_2} = \begin{cases} 0 \text{ if } i \in K \\ \\ \frac{\rho_i \sigma_i}{\sum_{j \in K^c} \rho_j \sigma_j} \big(1 + \frac{\gamma_1(n)}{\gamma_2(n)} \sum_{j \in K^c} \beta_j\big) - \frac{\gamma_1(n)}{\gamma_2(n)} \beta_i \text{ if } i \in K^c \end{cases} \tag{14}$$

for $i = 1, ..., m$.
The optimal variance obtained with this allocation is: $\sigma^2_{opt_2}/n$ with

$$\sigma^2_{opt_2} := \sum_{i \in K} \frac{\rho_i^2 \sigma_i^2}{\gamma_1(n)\beta_i} + \frac{1}{\gamma_2(n) + \gamma_1(n) \sum_{j \in K^c} \beta_j} \Big(\sum_{i \in K^c} \rho_i \sigma_i \Big)^2 \tag{15}$$

and we get the following variance inequality:

$$\sigma^2_{opt_1} \leq \sigma^2_{opt_2}. \tag{16}$$

2.2. ADS-2 estimator definitions and properties

Now, we have all the tools to set up our 2-steps adaptive method with an estimator coupling stratification and directional sampling. We will call this estimator the 2-adaptive directional stratification (ADS-2) estimator. It will be denoted by $\hat{I}^{ADS-2}$.

Let us explain our strategy. We split the total number n of draws into two parts: $\gamma_1(n)n$ and $\gamma_2(n)n$ such that $\sum_{i=1}^{2}\gamma_i(n) = 1$ and $(\gamma_i(n))_{i=1,2}$ are functions of the variable n. The first part, $\gamma_1(n)n$, will be used to estimate the optimal allocation minimizing the variance (learning step), and the second part, $\gamma_2(n)n$, will be used to estimate the failure probability (estimation step), using the estimation of the optimal allocation.

For instance, we can take $\gamma_1(n) = n^{l-1}$ with $l \in (0,1)$, or $\gamma_1(n) = \gamma_1$ with $\gamma_1 \in (0,1)$ and, in an obvious way, we have $\gamma_2(n) = 1 - \gamma_1(n)$. Let us set a prior choice of the draw proportions $(w_i)_{i=1,...,m}$ for the m strata we define as the quadrants of the Gaussian space. Without any other information, the most natural choice is a uniform allocation, $(w_i) = (\rho_i)$. Let us suppose we use the directional and stratification estimator (7). Consequently, the idea is to replace the allocation $(w_i)_{i=1,...,m}$ by an estimation, $(\tilde{W}_i)_{i=1,...,m}$, of the optimal allocation made with the $\gamma_1(n)n$ first draws: optimization problem results (10) and (14) are the optimal allocations on which we will refer.

But first, we need to define our estimators. Two possibilities can be considered: we can choose either a recycling estimator or a non-recycling estimator.

The recycling ADS-2 estimator

The recycling ADS-2 estimator uses the $\gamma_1(n)n$ first draws, that are used for the optimal allocation estimation step, for the expectation estimation:

$$\hat{I}_r^{ADS-2} = \sum_{i=1}^{m} \rho_i \frac{1}{N_i^r} \sum_{j=1}^{N_i^r} \xi(\mathbf{A}_j^i) \tag{17}$$

with

$$N_i^r := \lfloor \gamma_1(n) n w_i \rfloor + \left\lfloor \gamma_2(n) n \tilde{W}_i^r \right\rfloor, \tag{18}$$

$(w_i)_{i=1,...m}$ the prior allocation made in the optimal allocation estimation step and $(\tilde{W}_i^r)_{i=1,...,m}$ given by (14), substituting the $(\sigma_i)_{i=1,...,m}$ by an estimation of them, $(\tilde{\sigma}_i)_{i=1,...,m}$, given, for all $i \in \{1, ..., m\}$, by:

$$\tilde{\sigma}_i = \sqrt{\frac{1}{n_i - 1}\sum_{j=1}^{n_i} \xi(\mathbf{A}_j^i)^2 - \frac{1}{n_i(n_i-1)}\Big(\sum_{j=1}^{n_i} \xi(\mathbf{A}_j^i)\Big)^2} \tag{19}$$

with $n_i = \lfloor \gamma_1(n) n w_i \rfloor$. Consequently,

$$\tilde{W}_i^r = \begin{cases} 0 \text{ if } i \in \tilde{K} \\ \\ \dfrac{\rho_i \tilde{\sigma}_i}{\sum_{j \in \tilde{K}^c} \rho_j \tilde{\sigma}_j}\Big(1 + \dfrac{\gamma_1(n)}{\gamma_2(n)} \sum_{j \in \tilde{K}^c} w_j\Big) - \dfrac{\gamma_1(n)}{\gamma_2(n)} w_i \text{ if } i \in \tilde{K}^c \end{cases} \tag{20}$$

where $\tilde{K}$ and $\tilde{K}^c$ are also estimated replacing the $(\sigma_i)_{i=1,...,m}$ by the $(\tilde{\sigma}_i)_{i=1,...,m}$ in algorithm 1.

This estimator has the following bias due to the dependence of the optimal allocation estimation:

$$\mathbb{E}\big(\hat{I}_r^{ADS-2}\big) - I = -\sum_{i\in K^c} \frac{\rho_i\gamma_1(n)w_i\gamma_2(n)}{(\gamma_1(n)w_i+\gamma_2(n)w_i^{opt_2})^2} Cov\left(\xi(\mathbf{A}^i), \tilde{W}_i\right) + o(\frac{1}{n}). \quad (21)$$

The covariance term can be more precisely expressed. It is of the order of $\frac{1}{n}$ and depends on the first, second and third order moments of the $\xi\big(A^i\big)$, so that this bias cannot be efficiently estimated with a small number of simulations.
If we suppose that $\gamma_1(n) = \gamma_1$, then the variance of the ADS-2 recycling estimator can be expressed as:

$$\begin{aligned} Var\big(\hat{I}_r^{ADS-2}\big) &= \frac{1}{n}\sum_{i\in K}\frac{\rho_i^2\sigma_i^2}{w_i\gamma_1} \\ &+\frac{1}{n}\mathbb{E}\Big(\sum_{i\in\tilde{K}^c}\rho_i^2\sigma_i^2\frac{\gamma_2\tilde{W}_i^r}{(\gamma_1 w_i+\gamma_2\tilde{W}_i^r)^2}\Big) \\ &+\frac{1}{n}\frac{\gamma_1\sum_{i\in K^c}w_i}{\big(\gamma_2+\gamma_1\sum_{i\in K^c}w_i\big)^2}\Big(\sum_{i\in K^c}\rho_i\sigma_i\Big)^2 + o(\frac{1}{n}). \end{aligned} \quad (22)$$

Then, we can prove the asymptotical convergence of the estimator to a Gaussian distribution under two types of assumption. Firstly, if we suppose that $\gamma_1(n) \to 0$ and $\gamma_1(n)n \to +\infty$, then:

$$\sqrt{n}(\hat{I}_r^{ADS-2} - I) \xrightarrow[n\to+\infty]{\mathcal{L}} \mathcal{N}(0, \sigma^2_{opt_1}). \quad (23)$$

Secondly, if we suppose that $\gamma_1(n) = \gamma_1$, then:

$$\sqrt{n}(\hat{I}_r^{ADS-2} - I) \xrightarrow[n\to+\infty]{\mathcal{L}} \mathcal{N}(0, \sigma^2_{opt_2}). \quad (24)$$

The assumption $\gamma_1(n) = \gamma_1$ corresponds to our framework: indeed, as the number of calls to the failure function is limited, it is the most appropriate assumption. Also, the corresponding convergence result could be used to obtain the robustness of the method by estimating the confidence interval it offers. For this latter, we could use an estimation of the variance expression of the estimator proposed in (22) resulting in the following estimator:

$$\begin{aligned} \hat{\sigma}_r^2 &= \frac{1}{n}\sum_{i\in\tilde{K}}\frac{\rho_i^2\hat{\sigma}_{i,r}^2}{w_i\gamma_1} \\ &+\frac{1}{n}\sum_{i\in\tilde{K}^c}\rho_i^2\hat{\sigma}_{i,r}^2\frac{\gamma_2\tilde{W}_i^r}{(\gamma_1 w_i+\gamma_2\tilde{W}_i^r)^2} \\ &+\frac{1}{n}\frac{\gamma_1\sum_{i\in\tilde{K}^c}w_i}{\big(\gamma_2+\gamma_1\sum_{i\in\tilde{K}^c}w_i\big)^2}\Big(\sum_{i\in\tilde{K}^c}\rho_i\hat{\sigma}_{i,r}\Big)^2 \end{aligned} \quad (25)$$

with

$$\hat{\sigma}_{i,r} = \sqrt{\frac{1}{N_i^r - 1}\sum_{j=1}^{N_i^r} \xi(\mathbf{A}_j^i)^2 - \frac{1}{N_i^r(N_i^r-1)}\big(\sum_{j=1}^{N_i^r} \xi(\mathbf{A}_j^i)\big)^2}. \tag{26}$$

We can notice that, referring to the result (16), under the realistic assumption $\gamma_1(n) = \gamma_1$, the optimal standard deviation we achieve, σ_{opt_2}, will be larger than σ_{opt_1}.

The non-recycling ADS-2 estimator
The non-recycling ADS-2 estimator does not use the $\gamma_1(n)n$ first draws for the expectation estimation. It only uses the second part of draws, $\gamma_2(n)n$:

$$\hat{I}_{nr}^{ADS-2} = \sum_{i=1}^{m} \rho_i \frac{1}{N_i^{nr}} \sum_{j=1}^{N_i^{nr}} \xi(\mathbf{A}_{n_i+j}^i) \tag{27}$$

with

$$N_i^{nr} =: \left\lfloor \gamma_2(n) n \tilde{W}_i^{nr} \right\rfloor \tag{28}$$

and $(\tilde{W}_i^{nr})_{i=1,...,m}$ given by (10) replacing the (σ_i) by their estimations defined by (23).
Thus, for all $i \in \{i = 1, ..., m\}$:

$$\tilde{W}_i^{nr} = \frac{\rho_i \tilde{\sigma}_i}{\sum_{j=1}^{m} \rho_j \tilde{\sigma}_j}. \tag{29}$$

This estimator is unbiased: $\mathbb{E}\big(\hat{I}_{nr}^{ADS-2}\big) = I$. The variance of the ADS-2 non-recycling estimator is:

$$Var\big(\hat{I}_{nr}^{ADS-2}\big) = \frac{1}{\gamma_2(n)n}\mathbb{E}\Big[\big(\sum_{i=1}^{m} \rho_i \frac{\sigma_i^2}{\tilde{\sigma}_i}\big)\big(\sum_{j=1}^{m} \rho_j \tilde{\sigma}_j\big)\Big]. \tag{30}$$

We also get the following Gaussian asymptotical results. Firstly, if we assume that $\gamma_1(n) \to 0$ and $\gamma_1(n)n \to +\infty$, then:

$$\sqrt{n}(\hat{I}_{nr}^{ADS-2} - I) \xrightarrow[n\to+\infty]{\mathcal{L}} \mathcal{N}(0, \sigma_{opt_1}^2). \tag{31}$$

Secondly, if we assume that $\gamma_1(n) = \gamma_1$, then:

$$\sqrt{n}(\hat{I}_{nr}^{ADS-2} - I) \xrightarrow[n\to+\infty]{\mathcal{L}} \mathcal{N}(0, \frac{1}{1-\gamma_1}\sigma_{opt_1}^2). \tag{32}$$

We notice that we do not achieve the optimal standard deviation, $\sigma_{opt_1}^2$: we loose a factor $\gamma_1/(1-\gamma_1)$ of it, i.e. the obtained variance is $\sigma_{opt_1}^2/(1-\gamma_1) = \sigma_{opt_1}^2 + \sigma_{opt_1}^2\gamma_1/(1-\gamma_1)$. To get the confidence interval offered by this result, we can estimate the standard deviation (30) of the estimator by:

$$\hat{\sigma}_{nr}^2 = \frac{1}{\gamma_2(n)n}\Big(\sum_{i=1}^{m} \rho_i \tilde{\sigma}_{i,nr}\Big)^2 \tag{33}$$

with

$$\hat{\sigma}_{i,nr} = \sqrt{\frac{1}{N_i^{nr}-1}\sum_{j=1}^{N_i^{nr}} \xi(\mathbf{A}_j^i)^2 - \frac{1}{N_i^{nr}(N_i^{nr}-1)}\Big(\sum_{j=1}^{N_i^{nr}} \xi(\mathbf{A}_j^i)\Big)^2}. \tag{34}$$

Conclusion and choice of the estimator

In conclusion, the ADS-2 strategy concentrates the runs into the most important parts of the sample space, which results in an asymptotic optimal error variance.

When the number of simulations is limited, the most natural assumption will be to choose $\gamma_1(n) = \gamma_1$, in order to have a sufficient number of draws in both learning and estimation steps of the ADS-2 method. We will look for the optimum of this parameter in the following numerical studies.

Another point is to make a choice between the recycling and the non-recycling estimators. Intuitively, the first choice would be for the recycling one, since re-using the first step draws seems to be more efficient to estimate the failure probability. However, the problem is that this recycling estimator is biased and this bias is not easy to estimate with a limited number of simulations, which is discrepant with the robustness we are looking for. Consequently, the unbiased non-recycling estimator seems to be a better choice: even if we loose some factor in the standard deviation, we know exactly how much.

2.3. Numerical application

In this section, we test numerically the efficiency of the ADS-2 method on various examples. First, we study the behaviour of the ADS-2 method on academic examples. Then, it is applied to two realistic models: the flood and the nuclear reactor pressure vessel models, presented in section 1.1.

Hyperplane failure surfaces

Here, we essentially want to determine the behaviour of the ADS-2 method in the cases where the failure surface is: (a) concentrated only in one quadrant, (b) essentially concentrated in one quadrant but with some part running over other quadrants, (c) uniformly concentrated in several quadrants. So, we test respectively the ADS-2 method considering three hyperplane failure surfaces:

$$H_1 : \sum_{i=1}^{p} x_i = k_1, \quad H_2 : \frac{1}{4}x_1 + \sum_{i=2}^{p} x_i = k_2, \quad H_3 : x_p = k_3,$$

with p the physical space dimension. To determine the constant k_j corresponding to a given failure probability, P_f, we just need to calculate some appropriate Gaussian quantiles.

Denoting by b the radius of the sphere beyond which the probabilities are insignificant in comparison with the seeked failure probability, it is defined in the p-dimensional Gaussian space by: $b = \sqrt{\chi^{-1}_{2,p}(1-\epsilon P_f)}$, with $\chi^{-1}_{2,p}$ the inverse chi-square probability distribution with p degrees of freedom and ϵ some margin, for example $\epsilon = 10^{-1}$. We want to study numerically the behaviour of the ADS-2 estimators on several configurations. The failure probability takes its values into: $P_f \in \{10^{-4}, 10^{-8}\}$, the physical space dimension takes its values into: $p \in \{3, 5, 8\}$, the percentage of directional draws allocated in the first step of the ADS-2 method, γ_1, takes its values between 5% and 85%:

$$\gamma_1 \in \{5\%, 10\%, 15\%, 25\%, 50\%, 75\%, 85\%\}$$

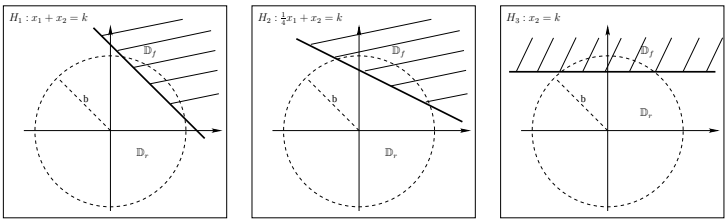

Fig. 2.2 Two dimensional graphic representations of respectively H_1, H_2 and H_3.

and the total number of directional draws, n, takes its values between 100 and 5000:

$$n \in \{100, 120, 140, 160, 180, 200, 240, 260, 280, 300, 500, 750, 1000, 1250, 1500, 2000, 3500, 5000\}.$$

From now on, until specific notification, the physical space dimension is $p = 3$. The quality of the ADS-2 estimators is evaluated through 4 indicators, depending of n and estimated over $N = 5000$ runs of the method. The 4 indicators are:

- the mean number of calls to the failure function G: $NG = \dfrac{1}{N}\displaystyle\sum_{k=1}^{N} NG_k$, with NG_k the number of calls to the failure function at the k-th run of the method
- the mean relative bias of the failure probability estimator: $\hat{B} = \dfrac{1}{N}\displaystyle\sum_{k=1}^{N} \hat{B}_k$, with $\hat{B}_k = \dfrac{\hat{I}_k^{ADS-2} - P_f}{P_f}$
- the mean coefficient of variation: $\hat{CV} = \dfrac{1}{N}\displaystyle\sum_{k=1}^{N} \dfrac{\hat{\sigma}_{nr,k}^{ADS-2}}{\hat{I}_k^{ADS-2}}$
- the percentage of estimations fallen in the estimated two-sided symmetric 95% confidence interval: $\hat{PCI} = \dfrac{100}{N}\displaystyle\sum_{k=1}^{N} \mathbb{1}_{P_f \in [\hat{P}_k^-; \hat{P}_k^+]}$, with $\hat{P}_k^{\pm} = \hat{I}_k^{ADS-2} \pm \alpha_{97,5\%} \dfrac{\hat{\sigma}_k^{ADS-2}}{\sqrt{n}}$, where $\alpha_{97,5\%}$ is the $97,5\%$ Gaussian quantile.

The figures of these 4 indicators are presented in Appendix B.

Figures 1 and 5 give the averaged number of calls to the failure function, NG, depending on n, when the seeked failure probability is respectively $P_f = 10^{-4}$ and 10^{-8}. NG goes from 3 to 10 in function of γ_1 and, of course, it increases linearly with n. The difference between the recycling and the non-recycling estimators is not significant. We can notice that when the failure function is concentrated in one quadrant (H_1), the number of calls is higher because the majority of the directional draws intersects the failure surface, which implies many calls to G due to the root-finding algorithm. On the contrary, when the failure surface stretches in multiple quadrants (H_3), a non negligible number of draws is lost and NG decreases. Moreover, when the seeked failure probability decreases, the mean number of calls to the failure function in one direction also decreases.

Figures 2 and 6 give an estimation of the relative bias, $\hat{B}$, of the ADS-2 estimators, depending on n, when the seeked failure probability is respectively $P_f = 10^{-4}$ and 10^{-8}. For the non-recycling estimator, the bias is clearly negligible and corresponds to the root-finding error. But for the recycling estimator, a substantial bias appears in the "worst cases" (multiple important quadrants). For example, with hyperplane H_3, the bias is of the order of magnitude of 20 to 30% of P_f. We can also observe that to minimize the bias when the failure surface is in several quadrants, we need to allocate enough simulations for the first step (learning step) of the method; 50% seems to be enough.

Figures 3 and 7 give an estimation of the coefficient of variation, $\hat{CV}$, of the ADS-2 estimators, depending on n, when the seeked failure probability is respectively $P_f = 10^{-4}$ and 10^{-8}. The estimation is made by approximating the variance expression of the ADS-2 estimators by $\hat{\sigma}^2_{nr}$. The dashed graphics correspond to the estimation of the relative standard deviation of the ADS-2 estimator by directly calculating the standard deviation with the $N = 5000$ iterations made. We can notice that the recycling estimator gives a smaller standard deviation in comparison with the non-recycling estimator. The bias, difference between the dashed and the solid lines, is also a little smaller, in particular for multiple quadrants failure surfaces. For both estimators, it is clear that the allocation γ_1 must be larger than 50%, as the standard deviation is smaller and the bias decreases quite quickly. The best compromise seems to be 50%. In this case, the sensitivity to the failure probability is negligible, otherwise it increases when the failure probability decreases.

Figures 4 and 8 give the percentage of estimations fallen in the estimated two-sided symmetric 95% confidence interval, $\hat{PCI}$, depending on n, when the seeked failure probability is respectively $P_f = 10^{-4}$ and 10^{-8}. Globally, the non-recycling estimator gives better results in comparison with the recycling one. The theoretical 95% confidence interval is also more difficult to achieve when the failure surface is in several quadrants. It is reached quite quickly for H_1, but when the failure surface extends into multiple quadrants (H_3), the inflation of the required simulations can be significant.

These numerical results bring us to confirm the existence of the bias of the recycling estimator. This recycling estimator gives quite better results for the standard deviation estimation in the cases of multiple quadrants failure surfaces, but it is also in these configurations where the bias is consequent. As we have theoretically seen in section 2.2, we loose some precision (and we know exactly how much) with the non-recycling estimator; however, this latter is much more reliable. This fact appears clearly in the graphics presenting the percentage of estimations fallen in the estimated confidence interval (Figures 4 and 8). Also, we have noticed that the best compromise for the allocation of simulations in the first step of the method, γ_1, is 50%, in order to estimate accurately the optimal allocation used in the second estimation step and thus keep a sufficient number of simulations for the final estimation of the failure probability. We numerically confirmed the asymptotic variance result (35), which gives a Gaussian control over the estimation error, as shown in the following Figure 3.2.

Summarizing, we confirmed numerically: the consistency of both recycling and non-recycling estimators, the bias of the recycling estimator and the lack of this bias for the non-recycling estimator, the theoretical Gaussian behaviour of the standard deviation of both estimators and the control of the error estimation for both recycling and non-recycling estimators. We determined that, empirically, the best γ_1 is about 50% for a limited number of calls to the failure function and that the non-recycling estimator is more reliable than the recycling one, because of the bias

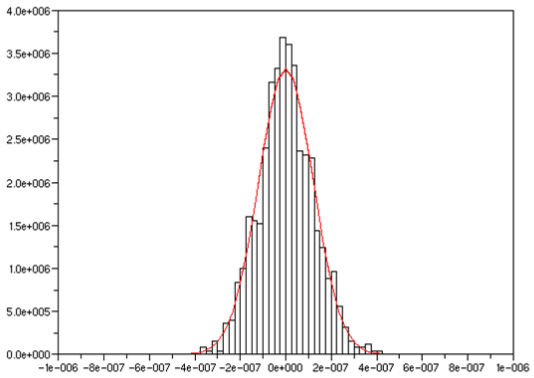

Fig. 2.3 Empirical histogram of the non-recycling ADS-2 estimator on H_1 with $p = 3$, $P_f = 10^{-7}$, $n = 1000$, $N = 1000$ and $\gamma_1 = 0.5$.

of this latter which can not be easily corrected. We noticed that the worst case is when the failure surface is uniformly distributed in several quadrants (H_3). In this case, the learning step of the method must be very important to obtain a reliable estimation of the optimal allocation. We have observed that the ADS-2 method is not very sensitive to the order of magnitude of the failure probability, although the efficiency decreases slowly with the failure probability. We recall that all the previous results have been obtained for a physical dimension $p = 3$. In the following, we study the behaviour of the ADS-2 estimators when the dimension increases. Intuitively, it is clear that, for a fixed number of simulations, the estimation deteriorates when the dimension increases. Indeed, the physical space becomes larger and the number of quadrants increases exponentially. A small number of simulations, as we have in practice for industrial cases, will not be enough to detect the failure surface accurately. In Figure 9 (Appendix B), we present the percentage of estimations fallen in the estimated two-sided symmetric 95% confidence interval for $p = 3, 5$ and 8.
We observe that, as the dimension increases, the result can be just less reliable when the hyperplane is concentrated in one quadrant (H_1), but when the surface is uniformly distributed in several quadrants (H_3), then the results are clearly not efficient at all. The impact of the extension of the surface over multiple quadrants is more reasonable when the dimension is about $p = 3$. Clearly, we need to control the dimension of the random inputs of the physical model and some reduction over it must be achieved before applying the ADS-2 method. When the random inputs are more than 3, a choice over which inputs to stratify should be advised: we will give a method for this selection in section 3.4.

The flood model

From now on, we only consider the non-recycling estimator, since we have seen in the previous section that it is the most appropriate to estimate small probabilities with a small number of calls to the failure function.

The flood model has been presented in section 1.1. We recall that this model takes into ac-

count 4 random variables. The failure probability is of the order of magnitude of 10^{-2}, which may be seen like an upper range for small failure probabilities. As many standard methods have been tested on this model to estimate the failure probability, it is an interesting model for benchmarking our ADS-2 method. We will denote MC the standard Monte-Carlo method, DR the dimension reduction method, DS the standard directional simulation method and IS the importance sampling method around the FORM/SORM design point (DP).
Table 2.1 gathers the coefficients of variation ($\hat{CV}$) obtained with these methods depending on the number of calls to the failure function, NG, and for $N = 1$.

Method	n	NG	$\hat{P}_f$	$\hat{CV}$ (%)
MC	10^4	10^4	0.85×10^{-3}	10.8
MC	10^5	10^5	1.14×10^{-2}	2.9
MC	10^6	10^6	1.16×10^{-2}	0.92
DR (Q)	10^4	10^4	1.16×10^{-3}	3.6
DR (Q)	10^5	10^5	1.19×10^{-2}	1.1
DR (Q)	10^6	10^6	1.17×10^{-2}	0.37
DR (K_s)	10^4	10^4	1.16×10^{-3}	4
DR (K_s)	10^5	10^5	1.17×10^{-2}	1.3
DR (K_s)	10^6	10^6	1.17×10^{-2}	0.41
DS	2700	$\approx 10^4$	1.13×10^{-2}	5.82
DS	27350	$\approx 10^5$	1.18×10^{-2}	1.87
DS	273500	$\approx 10^6$	1.18×10^{-2}	0.59
ADS-2	2850	$\approx 10^4$	1.17×10^{-2}	2.8
ADS-2	28000	$\approx 10^5$	1.20×10^{-2}	0.89
ADS-2	282000	$\approx 10^6$	1.17×10^{-2}	0.28
IS (DP)	10^4	10^4	1.19×10^{-3}	1.7
IS (DP)	10^5	10^5	1.18×10^{-2}	0.56
IS (DP)	10^6	10^6	1.19×10^{-2}	0.18

Table 2.1. Non-recycling ADS-2 estimator results compared with different simulation methods with the flood model. $N = 1$.

For the same number of calls to the failure function, the ADS-2 method gives much better coefficients of variation than the standard Monte-Carlo, the dimension reduction and the standard directional simulation methods. The importance sampling method gives smaller coefficients of variation, but these results are still dependent on the design point, the uniqueness of this one being not insured. So, the ADS-2 method gives a little larger $\hat{CV}$ in comparison with the importance sampling, but with robust results in addition. Also, we can notice that the ADS-2 method can be combined to the dimension reduction, as both methods are completely independent.
Table 2.2 gives a more exhaustive behaviour of the ADS-2 method applied to the flood model. We can notice that the ADS-2 method begins to stabilize when the number of calls to the failure function is around $NG = 800$: then, the coefficient of variation decreases, as predicted by the theory, at the rate $1/\sqrt{n}$. Besides, the simulations have been achieved with the same kernel and, even if in this example we underestimate the failure probability for the first values of n, the two-sided symmetric 95% confidence interval contains the real failure probability anyway.

Method	n	NG	$\hat{P}_f^{ADS-2}$	$\hat{CV}$ (%)
ADS-2	120	494	9.46×10^{-3}	24.4
ADS-2	160	592	1.02×10^{-2}	14
ADS-2	200	742	9.08×10^{-3}	12.2
ADS-2	240	870	9.07×10^{-3}	11.4
ADS-2	280	1060	1.01×10^{-2}	9.2
ADS-2	300	1110	1.14×10^{-2}	8.5
ADS-2	500	1790	1.20×10^{-2}	6.2
ADS-2	750	2654	1.22×10^{-2}	5.5
ADS-2	1000	3756	1.37×10^{-2}	4.8

Table 2.2. Non-recycling ADS-2 estimator results with the flood model for small values of n. $N = 1$.

The nuclear reactor pressure vessel model

The nuclear reactor pressure vessel model has been presented in section 1.1. As the failure event is conditional to a postulated thermal shock, all the following failure probability results must be multiplicated by the frequency of the shock event, which is very small ($\leq 10^{-4}$). We recall that the numbers of random inputs are 3, 5 and 7. We apply the ADS-2 method to estimate the failure probability and compare its results with the ones obtained with the standard directional simulation (DS) and the FORM/SORM methods. The computations have been performed with the platform OpenTURNS [25]. For the DS method, the root-finding algorithm is the standard dichotomic method. However, the dichotomic algorithm used in the ADS-2 method is computed with the stop criterion presented in section 3.1.

For $p = 3$, in table 2.3, we notice an improvement with the use of the ADS-2 method:

- with a similar number of calls to the failure function, the ADS-2 failure probability estimation is slightly better than the SORM result in order of magnitude talking. Moreover, we can notice the large difference between the FORM and SORM results which motivates our method, that offers a confidence interval and thus provides a controlled estimation.
- in comparison with DS, for a same number of calls to the failure function, G_{Min}, the ADS-2 method gives a better estimation of P_f and reduces the width of the two-sided symmetric 95% confidence interval.
- in comparison with DS, for a same coefficient of variation (i.e. a comparable estimation error), the ADS-2 method enables to reduce the number of calls to G_{Min} by a factor of about 3.

Method	n	NG	$\hat{P}_f$	$\hat{CV}(\%)$
ADS-2	100	593	2.3×10^{-6}	35
ADS-2	140	918	5.1×10^{-6}	26
ADS-2	180	1169	5.3×10^{-6}	21
ADS-2	220	1371	4.3×10^{-6}	20
ADS-2	260	1446	4.1×10^{-6}	19
ADS-2	280	1632	3.8×10^{-6}	18.5
ADS-2	600	3832	4.5×10^{-6}	12.5
ADS-2	2000	12781	4.1×10^{-6}	7
DS	500	1553	6.1×10^{-6}	29
DS	1000	3116	8.0×10^{-6}	21
DS	5000	15103	5.45×10^{-6}	9.4
FORM	–	80	9.0×10^{-6}	–
SORM	–	1668	4.4×10^{-5}	–

Table 2.3. ADS-2 and DS results with the NRPV model. $p = 3$. $N = 1$.

Furthermore, in comparison with the DS method, as in the previous academic examples, when the dimension increases, we can expect a significant improvement of the ADS-2 results and the associated uncertainty. For a dimension $p = 5$, in table 2.4, taking as reference the results obtained with the largest number of simulations $n = 8192$, we can notice that the minimum number of calls to the failure function required to obtain a coherent result is larger than the one required when $p = 3$. It begins to stabilize for a number of calls around $NG = 6000$. It can be explained by the fact that a larger number of simulations is necessary to accurately detect the important strata.

Also, in comparison with the DS method, we can see that the gap between the two methods has increased. The number of calls needed to obtain a similar standard deviation with DS in comparison with ADS-2 is definitively prohibitive. Finally, we observe that the FORM calculation of the failure probability is strongly over-evaluated and that the SORM one is similar to the ADS-2 estimation. The numbers of calls to the failure function required by the FORM/SORM methods are small compared with the ADS-2 method. Nevertheless, the reliability of the results they provide is not insured, as we can see through the large difference between the FORM and the SORM evaluations of the failure probability. By contrast, the ADS-2 method is robust, since it supplies a confidence interval on the failure probability estimation.

Method	n	NG	$\hat{P}_f$	$\hat{CV}(\%)$
ADS-2	256	849	1.8×10^{-6}	95
ADS-2	512	1734	5.7×10^{-7}	53
ADS-2	1024	2848	2.0×10^{-7}	50
ADS-2	2048	6755	7.7×10^{-7}	53
ADS-2	4096	13203	4.8×10^{-7}	22
ADS-2	8192	23324	4.3×10^{-7}	20
DS	4096	9246	1.5×10^{-6}	65
DS	6144	13871	1.2×10^{-6}	56
FORM	–	132	6.6×10^{-4}	–
SORM	–	1688	7.2×10^{-7}	–

Table 2.4. ADS-2, DS and FORM/SORM results with the NRPV model. $p = 5$. $N = 1$.

In conclusion, for large dimensions, the number of simulations needed to obtain reliable results is clearly too large regarding our constraints. So, this point motivates the work presented in section

3.4, which proposes a solution to reduce the number of calls to the failure function when the dimension is larger than 3.

3. Improvement and monotonicity hypothesis

3.1. A stop criterion for the dichotomic algorithm in the directional sampling method: small failure probability case

Root-finding algorithms lead to numerical approximation errors that may strongly impact the estimation of the failure probability. Thus, the question is: how many steps do we have to perform to keep having the variance reduction result with the directional sampling method? Hence the necessity of an analysis on the propagation and the control of these errors. Thus, our purpose is to control the numerical error generated by the use of the chosen root-finding algorithm for a continuous and potentially monotonic failure function. We assume that the root is unique, which is true in some part of the physical space under monotonicity hypothesis.
The standard root-finding methods are the dichotomic, the secant, the inverse quadratic interpolation and the Brent methods. The secant and the inverse quadratic interpolation methods do not fit with our point of view, because they need additional hypotheses over the failure function to get an error control. Despite of the fact that it is not the fastest method, the dichotomic method has an error control without any additional assumption: so, it is a robust algorithm over which the error propagation can be studied. We can notice that the Brent method is designed to combine the reliability of the dichotomic method and the convergence speed of the secant and inverse quadratic interpolation methods. Consequently, in the implementation step, we will use the Brent method for which the errors studied for the dichotomic method still stand. In this section, we suppose that:

$$2 \leq p \leq 8 \qquad \text{and} \qquad P_f \leq 10^{-3} \tag{35}$$

and we focus on the dichotomic algorithm. Then, in this case, the directional simulation estimator becomes:

$$\hat{P}_f^{DS} = \frac{1}{n} \sum_{i=1}^{n} \left[1 - \chi_p^2(r_i^2)\right] \tag{36}$$

where r_i is the i-th root. We consider a bound, b, for the root beyond which the probabilities are insignificant in comparison with the failure probability to be estimated, so that the interesting roots are in the interval $[0, b]$. b can be determined by a quantile calculation. We can also consider a lower bound a under which the probability is larger than a prior estimation of the failure probability (considering that we are looking for a small probability): in the same way, a can be determined by a quantile calculation. We suppose that the dichotomic method is performed in the interval $[a, b]$. Let us denote by k_i the number of steps performed with the dichotomic method in the i-th direction to obtain the root r_i. We know that, at the step k_i, we obtain a solution interval $S_{k_i} = [A_{k_i}, B_{k_i}]$ with $|S_{k_i}| = B_{k_i} - A_{k_i} = (b-a)/2^{k_i}$ and r_i is somewhere within this interval. For the approximation of r_i in S_{k_i}, we choose the middle point of S_{k_i}: $r_i^\epsilon = (B_{k_i} + A_{k_i})/2$. Then, we model $r_i - r_i^\epsilon$ by ϵ_i^c, a uniform random variable over the interval $[-(b-a)/2^{k_i+1}, (b-a)/2^{k_i+1}]$, as we do not have more information on its location without

any other assumption. Thus, $r_i^\epsilon = r_i + \epsilon_i^c$. Now, we have the directional simulation estimator including the numerical approximation error:

$$\hat{P}_{f,\epsilon_c}^{DS} = \frac{1}{n}\sum_{i=1}^{n} 1 - \chi_p^2\big((r_i + \epsilon_i^c)^2\big). \tag{37}$$

Using Taylor expansions, we find the following results.
Under assumptions (39) and if

$$\min_{j=1,\dots,n}(k_j) \geq C(a,b,p) \tag{38}$$

with $C(a,b,p) =: \ln\big(\frac{(b-a)|p-1-b^2|}{b}\big)/\ln(2)$, then we have the following control over the bias:

$$\big|B(\hat{P}_{f,\epsilon_c}^{DS})\big| = \big|\mathbb{E}\big(\hat{P}_{f,\epsilon_c}^{DS}\big) - P_f\big| \leq \frac{(b-a)^2}{3n}\sum_{j=1}^{n}\frac{\psi(r_j^2)|p-1-r_j^2|}{2^{2k_j+2}} \tag{39}$$

and over the variance:

$$\big|Var\big(\hat{P}_{f,\epsilon_c}^{DS}\big) - Var(\hat{P}_f^{DS})\big| \leq \frac{(b-a)^2}{3n^2}\sum_{j=1}^{n}\frac{\big(\psi(r_j^2)r_j\big)^2}{2^{2k_j}}. \tag{40}$$

The variance result enables to look for the optimal allocation k_i which minimizes the number of calls to the failure function, G, and at the same time, allows to keep a control on the numerical error to the variance. For this, we solve the following optimization problem:

$$(E)\begin{cases} \min\limits_{(k_j)_{j=1,\dots,n}}\left(\sum\limits_{j=1}^{n} k_j\right) \\ \text{under the constraint:} \\ \dfrac{(b-a)^2}{3n^2}\sum\limits_{j=1}^{n}\dfrac{\big(\psi_p(r_j^2)r_j\big)^2}{2^{2k_j}} \leq s \end{cases} \tag{41}$$

with s a fixed threshold. Then, the solution is the sequence $(\overline{k}_j)_{j=1,\dots,n}$ defined by:

$$\overline{k}_j = \kappa(r_j) := \frac{\ln\big(\frac{(\psi(r^2)(b-a)r)^2}{3ns}\big)}{2\ln 2}. \tag{42}$$

We determine that assumption (42) is satisfied for:

$$s \leq \frac{\psi_p^2(b^2)b^4}{3n|p-1-b^2|^2}. \tag{43}$$

Hence, after these considerations, substituting (43) (replacing the inequality by an equality) into the expression of $\overline{k}_j$ (42), the optimal number of dichotomic steps which enables to keep a control over the numerical errors propagation to the variance estimator is defined, for $i \in \{1,...,n\}$, by:

$$k_i^{opt} = \kappa^{opt}(r_i) =: \ln\big(\frac{(\psi(r_i^2)r_i(b-a)|p-1-b^2|)^2}{(\psi_p(b^2)b^2)^2}\big)/[2\ln(2)]. \tag{44}$$

Finally, this result seems to be a priori useless from a practical point of view, since k_i^{opt} depends on r_i. Nevertheless, this result can contribute for the design of a stop criterion for the dichotomic

algorithm. As we denote by k_i the k-th step of the dichotomic research of the i-th root, we know that, at the step k_i, the dichotomic algorithm gives the solution interval $[A_{k_i}, B_{k_i}]$. Consequently, we have $r_i \in [A_{k_i}, B_{k_i}]$. Thus,

$$k_i^{opt} \in \left[\min\big(\kappa^{opt}(A_{k_i}), \kappa^{opt}(B_{k_i})\big), \max\big(\kappa^{opt}(A_{k_i}), \kappa^{opt}(B_{k_i})\big)\right],$$

which provides the following stop criterion.

Dichotomic method stop criterion:

The dichotomic method in the i-th direction should stop as soon as the k-th step of the dichotomic research of the i-th root satisfies:

$$k_i > \max\big(\kappa^{opt}(A_{k_i}), \kappa^{opt}(B_{k_i})\big)$$

with $\kappa^{opt}(r)$ given by (48).

3.2. Notation, definition and properties given by the monotonicity hypothesis

We consider a failure function G defined over $\mathbb{D} \subset \mathbb{R}^p$ and we recall that $\mathbb{D}_r$, $\mathbb{D}_f$ and $\mathbb{D}_l$ respectively represent the reliability domain, the failure domain and the limit state surface. Let us begin with specifying the monotonicity notion we consider. A function $f : \mathbb{R}^p \longrightarrow \mathbb{R}$ is globally monotonic if and only if $\forall i \in \{1, ..., p\}$, $\forall (x_1, ..., x_{i-1}, x_{i+1}, ..., x_p) \in \mathbb{R}^{p-1}$, $f_i : \mathbb{R} \to \mathbb{R}$, defined by $f_i(x_i) = f(x_1, ..., x_i, ...x_p)$, is a monotonic function. From now on, when we talk about the monotonicity hypothesis, we refer to the global monotonicity definition. To simplify the study, we also suppose that this monotonicity is decreasing, i.e all the functions f_i are decreasing. If the f_i are not all decreasing, a simple change of variable can put us in the considered case. So, we will equivalently say G is monotonic or G is decreasing.

We denote by $\preceq$ the partial order between elements of any p-dimensional space, i.e $\mathbf{x} \preceq \mathbf{y}$ (respectively $\mathbf{x} \succeq \mathbf{y}$) means that all components of $\mathbf{x}$ are together lower than (respectively upper than) or equal to the components of $\mathbf{y}$. Then, a negative hypercone of vertex $\mathbf{x} = (x_1, ..., x_p)$ or a negative $\mathbf{x}$-hypercone is the set defined by: $H_{\mathbf{x}}^- = \{\mathbf{y} \in \mathbb{D}, \quad \mathbf{y} \succeq \mathbf{x}\}$ and in the same way, a positive $\mathbf{x}$-hypercone is defined by: $H_{\mathbf{x}}^+ = \{\mathbf{y} \in \mathbb{D}, \quad \mathbf{y} \preceq \mathbf{x}\}$. These $\mathbf{x}$-hypercones are illustrated in Figure 3.1. In a general frame, the monotonicity hypothesis indicates that if $\mathbf{x} \in \mathbb{D}_f$,

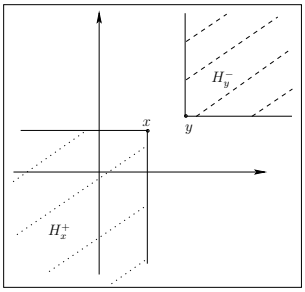

Fig. 3.1 Two-dimensional hypercone illustration.

then $H_{\mathbf{x}}^- \subset \mathbb{D}_f$, and if $\mathbf{x} \in \mathbb{D}_r$, then $H_{\mathbf{x}}^+ \subset \mathbb{D}_r$. These results express the fact that if a point $\mathbf{x}$, in the physical space, is in the reliability domain, then the positive $\mathbf{x}$-hypercone associated will also be in the reliability domain. Inversely, if $\mathbf{x}$ is in the failure domain, then the negative

$\mathbf{x}$-hypercone associated will be in the failure domain. Moreover, under monotonicity hypothesis, denoting $int(A)$ the largest open set included in A, if $\mathbf{x} \in \mathbb{D}_l$, then $\mathbb{D}_l \subset (int(H_{\mathbf{x}}^+ \cup H_{\mathbf{x}}^-))^c$. This result says that the limit state surface can be bounded by some unions of hypercones with their vertex on the limit state; furthermore, it can also be bounded just by some unions of hypercones whose vertex are not necessarily on the limit state.

3.3. Root-finding improvement using monotonicity

The algorithm

We assume that the failure function is monotonic. Then, applying the properties of the previous section, we can deduce an algorithm which enables for each direction to reduce the length of the interval used as prior for the dichotomy, using the solution intervals of the function G in this direction. The idea is to use the fact that after the application of the dichotomic root-finding algorithm in one direction, we obtain two bounds for the root. The left bound belongs to the safety domain and the right bound belongs to the failure domain. Let us consider the left one: then we know that the positive hypercone with vertex this left bound is in the safety domain. Now, if we make a dichotomic root-finding in another direction, then the straight line representing the new direction could have an intersection with the previous positive hypercone. If it is the case, we can begin the dichotomic algorithm not between 0 and b, but between, on the one hand, the intersection of the straight line and the positive hypercone and, on the other hand, b. The same analysis can be done with the other right bound. Also, this process can be reiterated taking into account, at each step, all the previous bounds already found. Figures 3.2 and 3.3 illustrate this idea. Consequently, the aim is to find the intersection between the straight line representing the current direction and the domains for which we are sure whether they are in the safety or in the failure domain thanks to the roots previously determined. Based on this idea, we propose the following dichotomic algorithm illustrated in Figure 3.1. Let us suppose we have already found

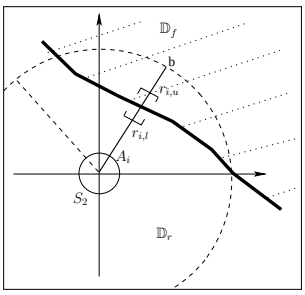

Fig 3.2 Two dimensional root-finding result illustration.

d solution intervals: $([r_{i,l}, r_{i,u}])_{i=1,\dots,d}$ in the directions $(\mathbf{A}_i)_{i=1,\dots,d}$. So, we have $2d$ points in $\mathbb{R}^p$:

$$(\mathbf{z}_{i,k})_{i=1,\dots,d}^{k\in\{l,u\}} \quad \text{with} \quad \mathbf{z}_{i,k} = \mathbf{A}_i r_{i,k}.$$

We build:

$$\mathbb{D}_d^+ = \bigcup_{i=1}^{d} D_i^+ \tag{45}$$

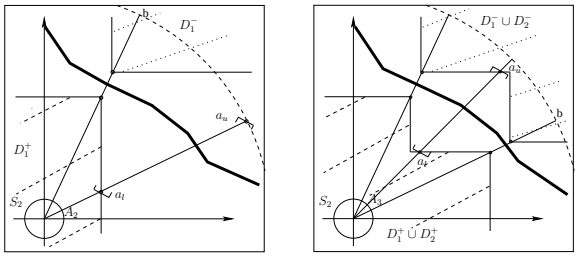

Fig 3.3 Two dimensional root-finding improvement illustration.

and

$$\mathbb{D}_d^- = \bigcup_{i=1}^{d} D_i^- \tag{46}$$

where $D_i^+ = H_{z_{i,l}}^+$ and $D_i^- = H_{z_{i,u}}^-$.
In the first direction $\mathbf{A}$ in which we have located a root (i.e. $G(\mathbf{A}b)G(0) < 0$), we denote $\mathbf{x}_0^+ = \mathbf{x}_0^- = 0$ and $\mathbf{y}_0^+ = \mathbf{y}_0^- = \mathbf{A}b$.
Then, at step $k \geq 1$:
on the one hand, if $(\mathbf{x}_k^+ + \mathbf{y}_k^+)/2 \notin D_d^+$, then

$$\mathbf{x}_{k+1}^+ = \mathbf{x}_k^+ \quad \text{and} \quad \mathbf{y}_{k+1}^+ = \frac{\mathbf{x}_k^+ + \mathbf{y}_k^+}{2},$$

else

$$\mathbf{x}_{k+1}^+ = \frac{\mathbf{x}_k^+ + \mathbf{y}_k^+}{2} \quad \text{and} \quad \mathbf{y}_{k+1}^+ = \mathbf{y}_k^+,$$

and, on the other hand, if $(\mathbf{x}_k^- + \mathbf{y}_k^-)/2 \in D_d^-$, then

$$\mathbf{x}_{k+1}^- = \mathbf{x}_k^- \quad \text{and} \quad \mathbf{y}_{k+1}^- = \frac{\mathbf{x}_k^- + \mathbf{y}_k^-}{2},$$

else

$$\mathbf{x}_{k+1}^- = \frac{\mathbf{x}_k^- + \mathbf{y}_k^-}{2} \quad \text{and} \quad \mathbf{y}_{k+1}^- = \mathbf{y}_k^-.$$

The number, t_a, of steps of the algorithm is not prohibitive, as we consider that the time required by the algorithm remains negligible in comparison with a call of the failure function. Finally, after l steps, we denote $\mathbf{a}_l = \mathbf{x}_{t_a}^+$ and $\mathbf{a}_u = \mathbf{y}_{t_a}^-$ and we set the root-finding over the interval $[\mathbf{a}_l, \mathbf{a}_u]$. We get a new solution interval, $[r_{d+1,l}, r_{d+1,u}]$. These two radius associated with the direction A give two new points which will be used to build D_{d+1}^+ and D_{d+1}^- and then we reiterate the algorithm in a new direction.

Numerical application
Here, we present the results obtained with the improved root-finding algorithm over the hyperplanes: H_1, H_2 and H_3. We numerically study the sensitivity of this algorithm to the dimension, p, the order of magnitude of the failure probability, P_f, and the type of hyperplane. For each

case, we display the new number of calls to the failure function G, New-NG, obtained with the improved algorithm, the previous number of calls to G, Prev. NG, obtained without and the percentage of reduction, denoted by Rd.
The results presented in tables 3.1, 3.2 and 3.3 make us notice that:

- for a fixed hyperplane, a fixed failure probability and a fixed n, the algorithm provides large percentages of reduction when the dimension is $p = 3$ and the efficiency strongly decreases for $p = 8$,
- for a fixed hyperplane, a fixed dimension and a fixed n, the sensitivity to the failure probability is not strong. We just observe that the percentage of reduction decreases with it,
- for a fixed hyperplane, a fixed dimension and a fixed failure probability, the percentage of reduction logically becomes better when n increases,
- for a fixed n, a fixed dimension and a fixed failure probability, the reduction of the number of calls is almost independent of the form of the hyperplane.

In conclusion, the improved root-finding algorithm is clearly adapted for a non too large dimension, but as the dimension increases, the gain becomes negligible. In the case of a small dimension, the reduction of the number of calls is non negligible, even for the limited number of calls we have. In our case, the percentage of reduction is between 15 to 20%.

p	P_f	n	New NG	Prev. NG	Rd (%)
3	10^{-4}	200	1098	1418	22.5
3	10^{-4}	500	2494	3336	25.2
3	10^{-6}	200	1150	1377	16.5
3	10^{-6}	500	2462	2974	17.2
3	10^{-8}	200	1127	1287	12.4
3	10^{-8}	500	2293	2640	13.1
8	10^{-4}	2000	13438	13660	1.6
8	10^{-4}	5000	28751	29350	2
8	10^{-6}	2000	16227	16335	0.6
8	10^{-6}	5000	35589	35978	1
8	10^{-8}	2000	16158	16228	0.4
8	10^{-8}	5000	37342	37508	0.4

Table 3.1. Improved root-finding algorithm results for hyperplane H_1.

p	P_f	n	New NG	Prev. NG	Rd (%)
3	10^{-4}	200	888	1163	23.6
3	10^{-4}	500	2006	2534	20.8
3	10^{-6}	200	907	1055	14
3	10^{-6}	500	1924	2403	20
3	10^{-8}	200	865	1005	14
3	10^{-8}	500	1900	2235	15
8	10^{-4}	2000	12322	12485	1
8	10^{-4}	5000	29182	29935	2.5
8	10^{-6}	2000	13092	13202	0.8
8	10^{-6}	5000	33165	33574	1.2
8	10^{-8}	2000	12191	12226	0.3
8	10^{-8}	5000	31490	31676	0.4

Table 3.2. Improved root-finding improvement algorithm results for hyperplane H_2.

p	P_f	n	New NG	Prev. NG	Rd (%)
3	10^{-4}	200	583	677	13.9
3	10^{-4}	500	1435	1903	24.6
3	10^{-6}	200	550	605	9
3	10^{-6}	500	1355	1679	19.3
3	10^{-8}	200	508	589	13.7
3	10^{-8}	500	1331	1562	14.8
8	10^{-4}	2000	5583	5706	2.1
8	10^{-4}	5000	12777	13541	5.6
8	10^{-6}	2000	5233	5274	0.8
8	10^{-6}	5000	11895	12118	1.8
8	10^{-8}	2000	4961	4966	0.1
8	10^{-8}	5000	11331	11448	1

Table 3.3. Improved root-finding improvement algorithm results for hyperplane H_3.

3.4. Improvement of the ADS-2 method for large dimensions

Classification of the influential random variables and stratification: the ADS-2^+ method

When the physical dimension grows, the number of strata of the ADS-2 method increases exponentially: indeed, in dimension p, the number of quadrants is 2^p. As a minimum of simulations is required to explore each quadrant, the number of directional simulations needed is too large for the restricted number of simulations we have. The idea is to get, with the simulations performed in the first step (learning step), a sort of the random variables in function of their influence on the failure event. Then, in the second step of the method (estimation step), we can only stratify the most important ones. To determine if a random variable will be stratified, we propose the following method. We first index the quadrants. The input index $k \in 1, ..., p$ is given the tag: i_k which takes its values in $\{-1, 1\}$ and corresponds to the input sign. Thus, each quadrant is characterized by a p-uple $(i_1, ..., i_p)$.

Then, we define the sequence $(T_k)_{k=1,...,p}$ by:

$$T_k = \sum_{i_l \in \{-1,1\}, l \neq k} \left| \tilde{P}(i_1, ..., i_{k-1}, -1, i_{k+1}, ..., i_p) - \tilde{P}(i_1, ..., i_{k-1}, 1, i_{k+1}, ..., i_p) \right| \quad (47)$$

with $\tilde{P}(i_1, ..., i_p)$ the estimation of the failure probability in the stratum $(i_1, .., i_p)$ obtained during the learning step.

Thus, T_k aggregates the differences of the failure probabilities between the quadrants along the dimension k. The larger T_k is, the more influential the k-th input is. Then, we sort the sequence $(T_k)_{k=1,...,p}$ by decreasing order and decide to stratify only over the $p' < p$ first dimensions, the other inputs being simulated without stratification. We have numerically showed in section 2.3 that, for the targeted number of simulations, the ADS-2 method is efficient when the number of random variables is close to 3. So a reasonable advice will be to take $p' = 3$. Then, in the second step of the method, we need to estimate the optimal allocation to be achieved in the new $m' = 2^{p'}$ hyper-quadrants. To do so, we still use the same formulas as the ones presented in section 2.2, for $i \in \{1, ..., m'\}$:

$$\tilde{W}_i^{nr+} = \frac{\rho_i^+ \tilde{\sigma}_i}{\sum_{j=1}^{m} \rho_j^+ \tilde{\sigma}_j} \quad (48)$$

with ρ_i^+ the failure probability of being in the i-th hyper-stratum and

$$\tilde{\sigma}_i = \sqrt{\frac{1}{n_i^+ - 1}\sum_{j=1}^{n_i^+}\xi(A_j^i)^2 - \frac{1}{n_i^+(n_i^+ - 1)}\Big(\sum_{j=1}^{n_i^+}\xi(A_j^i)\Big)^2} \tag{49}$$

with n_i^+ the number of simulations performed in the i-th hyper-stratum. Then, the new estimator is:

$$\hat{I}_{nr}^{ADS-2+} = \sum_{i=1}^{m'}\rho_i\frac{1}{N_i^{nr+}}\sum_{j=1}^{N_i^{nr+}}\xi(A_j^i) \tag{50}$$

with

$$N_i^{nr+} =: \left\lfloor \gamma_2(n) n \tilde{W}_i^{nr+} \right\rfloor. \tag{51}$$

The expression of the variance is:

$$Var\big(\hat{I}_{nr}^{ADS-2+}\big) = \frac{1}{\gamma_2(n)n}\mathbb{E}\Big[\Big(\sum_{i=1}^{m'}\rho_i'\frac{\sigma_i^{2+}}{\tilde{\sigma}_i^+}\Big)\Big(\sum_{j=1}^{m'}\rho_j'\tilde{\sigma}_j^+\Big)\Big] \tag{52}$$

with σ_i^+ the standard deviation of the i-th hyper-stratum and $\tilde{\sigma}_i^+$ its estimation. Of course, all the asymptotical results still stand. We will call this method the ADS-2^+ method.

We can remark that, under the monotonicity hypothesis, the shape of the failure surface is restricted: a symmetry or a quasi symmetry of the failure surface between two adjacent quadrants can appear only if at least one input has no or little influence on the failure. In this case, if we compare the failure probabilities between the quadrants along this dimension, they should be small. We can also indicate that we could have been more drastic and, after having determined the p' most important inputs, have set the other inputs to conservative values and achieved the ADS-2 method in the p'-dimensional space. This kind of strategy is a common practice in risk analysis, but if we make a wrong classification of the inputs with the statistics $(T_k)_{k=1,\dots,p}$, then we will set one (or several) influential input to a conservative value and the estimation of the failure probability might be too much conservative to be workable. Table 3.4 gives some results of this strategy, this conservative method being called CADS-2^+ and applied to the flood model.

Method	p'	n	NG	$\hat{P}_f$	$\hat{CV}$ (%)
CADS-2^+	2	256	1085	$9.5\ 10^{-2}$	6.5
CADS-2^+	2	512	2155	$8.5\ 10^{-2}$	4
CADS-2^+	3	256	1020	$2.3\ 10^{-2}$	7
CADS-2^+	3	512	2009	$2.0\ 10^{-2}$	5

Table 3.4. CADS-2^+ results with the flood model. $P_f = 1.17\ 10^{-2}$. $p = 4$. $N = 1000$.

The flood model has four random variables for inputs and we know that there are two influential inputs and two less influential ones (see Figure 3.6). As Table 3.4 shows, the estimations provided by the CADS-2^+ method are clearly conservative. We can propose an upper semi-confidence interval and the percentage of estimations fallen in this semi-confidence interval will be at 100%.

Another alternative is to keep simulating the $p - p'$ variables by a classical Monte-Carlo simulation: with this solution, then the problem is that we loose the directional strategy in the "eliminated" dimensions and as we are looking for small probabilities, this strategy dramatically reduces the estimation accuracy when there are more than p' influential inputs.

Numerical application to the hyperplanes
Here, we apply the ADS-2^+ method to hyperplanes H_1, H_3 and H_4, this latter being defined by

$$H_4 : \quad x_1 + 0.1x_2 + x_3 + 0.1x_4 + x_5 = k_4.$$

H_3 has one influential variable, H_4 three and H_1 has all its variables influential. We also apply ADS-2^+ to the flood and NRPV models presented in section 1.1.
For the hyperplanes results (tables 3.5 to 3.7), we have the following observations. The ADS-2^+ method gives similar results, in comparison with the ADS-2 ones, when the number of simulations is less than 500. But, when this number increases and is about 1000, which corresponds to approximatively 3000 calls to the failure function G, then the ADS-2^+ method gives more accurate estimations. We can also imagine that if the number of simulations is sufficiently large, the ADS-2 method, in which we consider more strata, will be again the best one. In other words, there is a interval of number of calls to G for which the ADS-2^+ is more efficient. This interval fortunately covers the number of calls we are limited to. More precisely, we can see that if there are exactly p' influential random variables, then the ADS-2^+ method is very significantly better than the ADS-2 even for a very small number of simulations. When there are less than p' important inputs, then we need a minimum of 3000 calls to G to ensure the accuracy of the estimations. Finally, when there are more than p' important random variables, which is the most penalizing situation for ADS-2^+, we do not deteriorate the percentage of estimations fallen in the two-sided symmetric 95% confidence interval, $\hat{PCI}$, which is a positive outcome. But we still need much more simulations to have the same coefficient of variation, $\hat{CV}$.

Method	n	NG	$\hat{P}_f$	$\hat{CV}$ (%)	$\hat{PCI}$
ADS-2^+	256	1075	$9.96\,10^{-5}$	25	92
ADS-2	256	1805	$9.71\,10^{-5}$	14	92
ADS-2^+	512	2100	$1.00\,10^{-4}$	19	90
ADS-2	512	3476	$1.02\,10^{-4}$	10	89
ADS-2^+	1024	4135	$1.02\,10^{-4}$	14	92
ADS-2	1024	6761	$1.01\,10^{-4}$	7	92

Table 3.5. ADS-2^+ and ADS-2 results with hyperplane H_1. $P_f = 10^{-4}$. $p = 5$. $p' = 3$. $N = 1000$.

Method	n	NG	$\hat{P}_f$	$\hat{CV}$ (%)	$\hat{PCI}$
ADS-2^+	256	783	$1.04\,10^{-4}$	62	61
ADS-2	256	891	$1.00\,10^{-4}$	59	67
ADS-2^+	512	1537	$9.77\,10^{-5}$	44	71
ADS-2	512	1626	$1.03\,10^{-4}$	52	70
ADS-2^+	1024	3065	$9.93\,10^{-5}$	29	86
ADS-2	1024	3117	$9.60\,10^{-5}$	39	72
ADS-2^+	2048	6113	$1.00\,10^{-4}$	18	92
ADS-2	2048	6150	$1.00\,10^{-4}$	26	86

Table 3.6. ADS-2^+ and ADS-2 results with hyperplane H_3. $P_f = 10^{-4}$. $p = 5$. $p' = 3$. $N = 1000$.

Method	n	NG	$\hat{P}_f$	$\hat{CV}$ (%)	$\hat{PCI}$
ADS-2^+	256	1198	$1.01\ 10^{-4}$	24	91
ADS-2	256	1323	$1.00\ 10^{-4}$	33	77
ADS-2^+	512	2397	$1.00\ 10^{-4}$	16	93
ADS-2	512	2516	$1.00\ 10^{-4}$	22	88
ADS-2^+	1024	4760	$1.00\ 10^{-4}$	11	94
ADS-2	1024	4920	$1.00\ 10^{-4}$	13	91

Table 3.7. ADS-2^+ and ADS-2 results with hyperplane H_4. $P_f = 10^{-4}$. $p = 5$. $p' = 3$. $N = 1000$.

As shown in table 3.8, when the failure probability decreases, the ADS-2^+ has approximatively the same improvement in comparison with ADS-2. However, we can notice the detrimental impact of the decrease of the failure probability over $\hat{PCI}$.

Method	n	NG	$\hat{P}_f$	$\hat{CV}$ (%)	$\hat{PCI}$
ADS-2^+	256	642	$1.03\ 10^{-8}$	88	35
ADS-2	256	772	$9.94\ 10^{-9}$	81	41
ADS-2^+	512	1278	$1.13\ 10^{-8}$	79	46
ADS-2	512	1387	$9.38\ 10^{-9}$	79	42
ADS-2^+	1024	2553	$9.60\ 10^{-9}$	59	58
ADS-2	1024	2634	$9.10\ 10^{-9}$	70	50

Table 3.8. ADS-2^+ and ADS-2 results with hyperplane H_3. $P_f = 10^{-8}$. $p = 5$. $p' = 3$. $N = 1000$.

We can also compare the results of the ADS-2^+ method when the number of insignificant random variables increases. For this, we define the new hyperplane:

$$H_5 : \quad x_1 + 0.1x_2 + x_3 + 0.1x_4 + x_5 + 0.1x_6 + 0.1x_7 = k_5.$$

Table 3.9 gives the comparison results. We observe that the increase of the dimension reduces the efficiency of the method. As the search space becomes larger, it is more difficult to find the failure surface. A significant part of the directional draws is "lost", consequently the mean number of calls to the failure function, NG, decreases, as $\hat{CV}$ and $\hat{PCI}$ proportionately.

Hyperplane	n	NG	$\hat{P}_f$	$\hat{CV}$ (%)	$\hat{PCI}$
H_5	1024	3184	10^{-6}	30	87
H_4	1024	4037	10^{-6}	20	93
H_5	2048	6411	10^{-6}	20	90
H_4	2048	8058	10^{-6}	10	94

Table 3.9. ADS-2^+ results with hyperplanes H_4 and H_5. $P_f = 10^{-6}$. $p = 5$. $p' = 3$. $N = 1000$.

Finally, we compare in table 3.10 the ADS-2^+ method with the Subset Simulation method (SS) which is built to overcome the curse of dimensionality and responds to the four constraints, presented in section 1.2, we want to deal with ([26]. Also, the results obtained with the ADS-2 method are presented. The SS results have been obtained using the open-source Matlab toolbox: FERUM (Finite Element Reliability Using Matlab) version 4.0.

Method	n	NG	$\hat{CV}$ (%)	$\hat{PCI}$
SS	500	3300	60	77
SS	700	4600	51	88
SS	1000	6700	42	81
ADS-2	1200	3219	55	61
ADS-2	1750	4675	46	61
ADS-2	2550	6760	39	76
ADS-2^+	1200	3139	41	78
ADS-2^+	1800	4799	31	83
ADS-2^+ ($p' = 1$)	1500	3957	28	92
ADS-2^+ ($p' = 2$)	1500	3962	30	90

Table 3.10 Results with hyperplane $\bar{H}_3$. $P_f = 10^{-6}$. $p = 5$. $p' = 3$. $N = 100$.

Table 3.10 confirms the efficiency of the ADS-2^+ method in comparison with the ADS-2 method. Moreover, in comparison with the SS method and for approximatively a same $\hat{CV}$ and $\hat{PCI}$, the ADS-2^+ method ($p' = 3$) enables to reduce the number of calls to the failure function by approximatively a factor 2. Also, for a better choice of p' (equal to 1 or 2), we can reduce the $\hat{CV}$ of 25% for approximatively the same number of calls to the failure function. As previously demonstrated in section 2.3, we emphasis the fact that hyperplan H_3 corresponds to the worst case for the ADS-2 and ADS-2^+ ($p' = 3$) methods. Finally, the same study has been performed on H_1 and H_3 for p going from 5 to 8 and $P_f = 10^{-6}$ and 10^{-8}. As predictable, the SS method is completely robust with respect to the increase of the dimension and gives almost exactly the same results. On H_1, the ADS-2 method always outperforms the SS method: for instance in dimension 7 for a failure probability of 10^{-8}, we divide by a factor 2 the $\hat{CV}$ with the half number of calls to the failure function used for SS (8000) while keeping a good $\hat{PCI}$. In the worst case, i.e. H_3, $P_f = 10^{-8}$ and $p = 7$, the results between SS and ADS-2^+ are equivalent.

Numerical application to the flood model

Table 3.11 presents the results obtained with the ADS-2^+ and ADS-2 methods for the flood model with $p' = 2$. We can remark that $\hat{PCI}$ and $\hat{CV}$ are quite similar for both methods, but if we look more carefully, we notice that the ADS-2^+ results are more robust for the smaller number of simulations. We can deduce that for $p = 4$, the ADS-2 method remains efficient as long as the physical space and the number of quadrants are not too large and ADS-2^+ is a little more reliable for very small numbers of simulations.

Method	n	NG	$\hat{P}_f$	$\hat{CV}$ (%)	$\hat{PCI}$
ADS-2	256	957	1.16×10^{-2}	10.2	92
ADS-2	512	1862	1.20×10^{-2}	7	94
ADS-2	1024	3670	1.17×10^{-2}	4.3	96
ADS-2	2048	7300	1.18×10^{-2}	3.4	94
ADS-2^+	256	895	1.18×10^{-2}	11.2	95
ADS-2^+	512	1784	1.19×10^{-2}	7.8	94
ADS-2^+	1024	3556	1.17×10^{-2}	5.4	93
ADS-2^+	2048	7100	1.18×10^{-2}	3.8	95

Table 3.11. ADS-2^+ and ADS-2 results with the flood model. $p = 4$ and $p' = 2$. $N = 1000$.

The vector $T := (T_k)_{k=1,\dots,p}$ gives a hierarchy of the p random variables. In the flood example, we know that there are two physical important random variables: (Q, K_s), and two less important: (Z_v, Z_m). Figure 3.4 presents the FORM importance factors. Then Figure 3.5 shows the

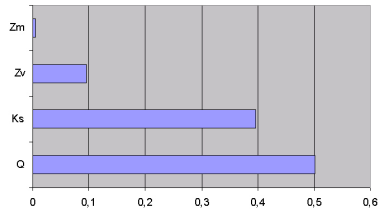

Fig. 3.4 FORM importance factor for the flood model.

distribution of the $p' = 2$ selected variables by T. We notice that the statistic T selects well the two most important inputs with high frequency. In this example, T seems to be an efficient statistic. Table 3.12 gives the results of the T-selection for hyperplane H_4. The percentage of

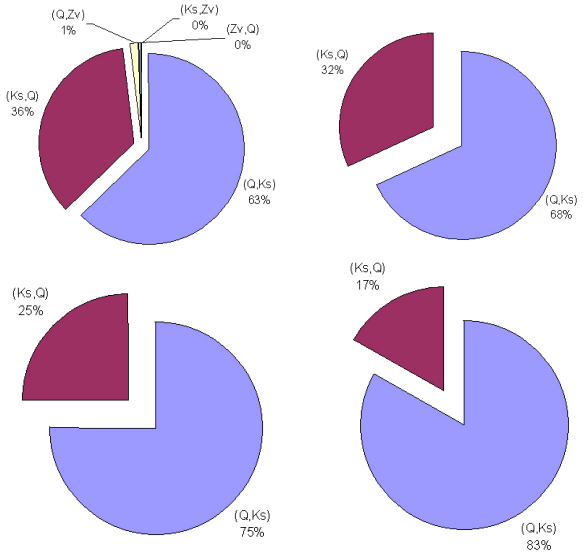

Fig 3.5 Percentage of the T-selection of the $p' = 2$ influential variables. $p = 4$. From left to right, n is equal to 256, 512, 1024 and 2048. $N = 1000$.

selection of the three most important variables, i.e. the first, the third and the fifth, is presented. Once again, the accuracy of the selection method is reasonable for a limited number of calls to the failure function.

n	NG	T_k-selection (%)
256	997	83
512	2033	99.5
1024	4037	100

Table 3.12. Percentage of the correct T-selection of the $p' = 3$ influential variables for H_4. $p = 5$. $P_f = 10^{-6}$. $N = 1000$.

Besides, the same results are obtained when we apply the T-selection method to hyperplanes H_1, H_2 and H_3.

Numerical application to the NRPV model

Now, we apply the ADS-2^+ method to the NRPV model. To begin with, we compare the organization into a hierarchy result given by the T-selection with the FORM one for a five-dimensional space. Figure 3.6 gives the classification obtained with the FORM method and the vector T. We remark that the selection of the $p' = 3$ important variables is the same with both methods. Nonetheless, the two less influential variables are not classified the same way. Indeed, for a small number of simulations, the statistic T only globally separates the real important variables from the negligible ones. Next, we compare the ADS-2^+ method with the ADS-2 method. The

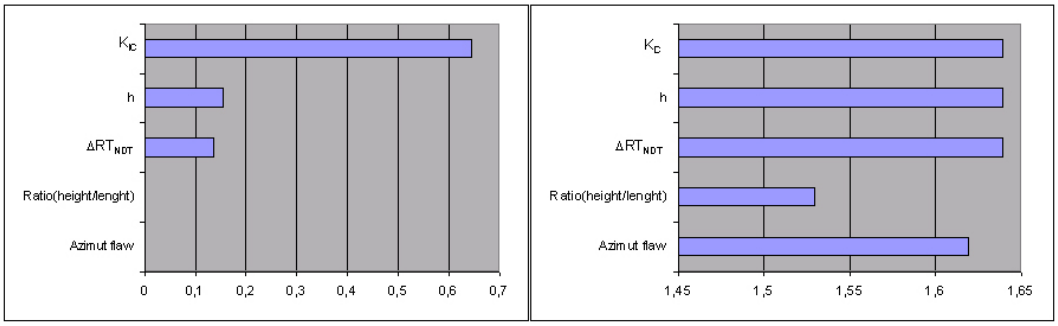

Fig. 3.6 FORM (left) and T-selection (right) results for the NRPV model with $p = 5$.

ADS-2^+ method applied to the NRPV model gives better results than the ADS-2 method. We can notice in table 3.13 that, for too small numbers of simulations, the results are not consistent. Then, the two methods stabilize and for the same number of calls to the failure function, $NG \approx 3000$, the methods give similar correct results. But for the same precision, it seems clear that the ADS-2 method requires fewer calls. Thus, we confirm the results obtained with hyperplane H_1: for the same reasonable number of calls to the failure function, we obtain a more reliable confidence interval with the ADS-2^+ estimator than with the ADS-2 estimator.

Method	n	NG	$\hat{P}_f^{ADS-2}$	$\hat{CV}$ (%)
ADS-2	256	849	1.8×10^{-6}	95
ADS-2	512	1734	5.7×10^{-7}	53
ADS-2	1024	2848	2.0×10^{-7}	50
ADS-2	2048	6755	7.7×10^{-7}	53
ADS-2	4096	13203	4.8×10^{-7}	20
ADS-2	8192	23324	4.3×10^{-7}	20
ADS-2^+	256	905	1.2×10^{-7}	43
ADS-2^+	512	1325	1.2×10^{-7}	57
ADS-2^+	1024	3036	6.1×10^{-7}	48
ADS-2^+	2048	4679	5.3×10^{-7}	38

Table 3.13. ADS-2^+ and ADS-2 results with the NRPV model. $p = 5$. $p' = 3$. $N = 1$.

So, the ADS-2^+ method increases the number of times we correctly get in the two-sided symmetric 95% confidence interval, but in compensation, the confidence interval gets larger when the number of influential (or non negligible) inputs is greater than the number of "kept" inputs p'.

4. Conclusion and perspectives

To overcome the main industrial constraints involved by the estimation of a small structural failure probability with a computationally expensive model (for example a nuclear reactor pressure vessel failure probability estimation), we have developed the new accelerated Monte-Carlo ADS-2 method. For a physical space dimension less than or equal to 4, the ADS-2 method enables to get a reliable confidence interval of the failure probability with a limited number of calls to the failure function (a few thousands). This number of calls is reduced by at least a factor 3 in comparison with the directional simulation. For a same number of calls to the failure function, the order of magnitude of the failure probability estimation is better or quite similar to a FORM/SORM result, and, additionally, it is reliable. When the dimension is larger than or equal to 5, as the number of strata increases exponentially and the physical space gets wider, the ADS-2 does not give robust results anymore, i.e. the percentage of estimations fallen in the two-sided symmetric 95% confidence interval ($\hat{PCI}$) is far from 95%. So, to counter the curse of dimensionality, we developed the ADS-2^+ method based on the basic ADS-2 method and on a statistical test to detect the most significant inputs, which then enables to reduce the number of dimensions along which the stratification is carried out. The $\hat{PCI}$ is improved in most cases. Also, the statistical test seems to be efficient for the number of calls we are limited to: for a small number of calls to the failure function, in comparison with the ADS-2 method, the ADS-2^+ method improves the $\hat{PCI}$ for a space dimension up to 7 (although we can notice that the confidence interval is a little larger). This improvement depends on the number of significant inputs: if it is larger than the number of inputs p' along which stratification is carried out (we propose $p' = 3$), then the improvement can be negligible in the worst case. When p' matches exactly the number of significant inputs, the improvement is substantial. Monitoring p' with respect to statistical test should be interesting. For a dimension greater than or equal to 7, the number of simulations required for the first learning step of the ADS methods is too large regarding the limited number of calls we have, and thus the $\hat{PCI}$ collapses. Another option is the CADS-2^+ estimator we proposed: no matter how many inputs we have, we set the $p - p'$ non-influential random variables we selected to deterministic and conservative values in order to

get a conservative 100% semi-confidence interval. However, the result can be distant from the real failure probability if the real number of influential variables is too far from p'. Finally, we compare the ADS-2 and ADS-2^+ methods to the subset simulation method which is one of the most relevant method to use in the context described in section 1.2. The results show that the ADS-2^+ method outperforms the subset simulation method. Hence, the ADS methods are very efficient when the following conditions are met: a number of calls to the failure function of a few thousand, an order of magnitude of the failure probability less than 10^{-4}, a dimension less than 7, no regularity assumption on the failure function, and a need for explicit and trustworthy error controls.

To summarize, the methods we have proposed respond substantially to the initial constraints for a realistic space dimension. To our opinion, it may not be unreasonable to concentrate onto at most half a dozen important variables when looking for improved accuracy in the prediction of rare failure probabilities. For larger sets of uncertain variables that may be involved in upstream stages of risk analysis, undertaking prior physical or numerical sensitivity studies may prove more relevant; remember also that the accuracy in the computation of failure probability makes sense only if there is high confidence in the description of the input uncertainty distributions. Finally, assuming that there is only one root in each direction, we got an "intelligent" stop criterion for the dichotomic root-finding algorithm, in order to keep the variance reduction result despite of the numerical error. Moreover, under the monotonicity hypothesis, we have proposed an algorithm to reduce the number of calls to the failure function in the root-finding step, by using the estimators of the previously determined roots. Thus, we reduced the number of calls to the failure function by 15 to 20% for a limited number of calls and a dimension less than or equal to 4.

A perspective would be to theoretically study the statistical test, T, in order to be able to estimate efficiently the number of significant inputs, also a quite similar strategy, with a different statistic, has been achieved in ([27]) and both methods could be compared. Another point would be to work on the first learning step of the method to make more accurate the detection of the important strata for a limited number of calls to the failure function. Firstly, we could think about a directional quasi Monte-Carlo approach or a directional and orthogonal sampling ([28]), in order to probe more efficiently the physical space in the first step and then, in the second one, better concentrate the directional draws in the detected influential parts. Secondly, to get a more accurate idea of the variation of the estimated allocation, we could use a bootstrap method. Finally, in order to better capture the failure area and the influential inputs, we could imagine an hybridization of the ADS methods with the FORM/SORM one, as this latter, for a small number of calls to the failure function, gives important information.

References

[1] H.O. Madsen and O. Ditlevsen. *Structural reliability methods*. Wiley, 1996.

[2] R. Rackwitz. Reliability analysis - a review and some perspectives. *Structural Safety*, 23, 2001.

[3] H. Riesch-Oppermann and A. Brckner-Foit. First- and second-order approximations of failure probabilities in probabilistic fracture mechanics. *Reliability Engineering & System Safety*, 23, issue 3:183–94, 1988.

[4] E. de Rocquigny. Structural reliability under monotony: properties of form, simulation or response surface methods and a new class of monotonous reliability methods (mrm). *Structural Safety*, 31:363–374, 2009.

[5] E. de Rocquigny, Y. Chevalier, S. Turato, and E. Meister. Probabilistic assessments of the reactor pressure vessel structural integrity: direct coupling between probabilistic and finite-element codes to model sensitivity to key thermo-hydraulic variability. In *ICONE12 congress*, 2004.

[6] C. Lemaignan. *Science des matériaux pour le nucléaire*. EDP Sciences, 2004.

[7] R.Y. Rubinstein and D.P. Kroese. *Simulation and the Monte-Carlo Method (second edition)*. Wiley, 2007.

[8] A. Gille-Genest. *Utilisation des methodes numeriques probabilistes dans les applications au domaine de Fiabilite des structures*. PhD thesis, University of Paris VI, 1999.
[9] C. Cannamela. *Apport des methodes probabilistes dans la simulation du comportement sous irradiation du combustible particules*. PhD thesis, University of Paris VII, 2007.
[10] HJ. Bungartz and S. Dirnstorfer. Multivariate quadrature on adaptive sparse grids. *Computing*, 71:89–114, 1985.
[11] T. Gerstner and M. Griebel. Numerical integration using sparse grids. *Numer. Algorithms*, 18:209–232, 1998.
[12] T. Gerstner and M. Griebel. Dimension-adaptive tensor-product quadrature. *Computing*, 71(1):65–87, 2003.
[13] H.O. Madsen, S. Krenk, and N.C. Lind. *Methods of structural safety*. Odile Jacob, 2000.
[14] J.C. Helton. Uncertainty and sensitivity analysis techniques for use in performance assessment for radioactive waste disposal. *Reliability Engineering & System Safety*, 42, issues 2-3:327–47, 1993.
[15] W.G. Cochran. *Sampling techniques (third edition)*. Wiley, 1977.
[16] P. Zhang. Nonparametric importance sampling. *J. Am. Stat. Assoc*, 91(435):1245–53, 1996.
[17] BD. Ripley. *Stochastic simulation*. New York: Wiley, 1987.
[18] D. Siegmund. Importance sampling in the monte-carlo study of sequential tests. *Anals stat*, 4:673–84, 1976.
[19] J.C. Helton, F.J. Davis, and J.D. Johnson. A comparison of uncertainty and sensitivity analysis results obtained with random and latin hypercube sampling. *Reliability Engineering & System Safety*, 89, issue 3:305–30, 2005.
[20] C. Cannamela, J. Garnier, and B. Iooss. Controlled stratification for quantile estimation. *Annals of Applied Statistics*, 2:1554–1580, 2008.
[21] P. Etore and B. Jourdain. Adaptive optimal allocation in stratified sampling methods. *Methodology and Computing in Applied Probability*, 2009.
[22] O. Ditlevsen, R.E. Melchers, and H. Gluver. Probability integration by directional simulation. *Journal of Eng. Mech.*, 36:355–68, 1990.
[23] P. Bjerager. Probability integration by directional simulation. *Journal of Eng. Mech.*, 114:1285–1302, 1988.
[24] R.B. Nelsen. *An introduction to copulas*. Springer, 1999.
[25] http://www.openturns.org.
[26] S.-K. Au and J.L. Beck. Estimation of small probabilities in high dimensions by subset simulation. *Probabilistic Engineering Mechanics*, 16:263–277, 2001.
[27] H. Chernoff, S-H. Lo, and T. Zheng. Discovering influential variables: a method of partitions. *Annals of Applied Statistics*, Vol. 3, No. 4:13351369, 2009.
[28] C. Tong. Refinement strategies for stratified sampling methods. *Reliability Engineering & System Safety*, 91, issue 10-11:1257–65, 2006.

Appendix A: Distributions formulas

Distribution	Parameters	Probability density function	Support
Gaussian	μ, σ	$\frac{1}{\sigma\sqrt{2\pi}} \exp\left(-\frac{1}{2}\left(\frac{x-\mu}{\sigma}\right)^2 \right)$	$(-\infty; +\infty)$
Gumbel	a, b	$\frac{1}{b} \exp(-\frac{x-a}{b}) \exp\left(-\exp(-\frac{x-a}{b}) \right)$	$(-\infty; +\infty)$
Triangular	a, b, c	$\frac{2(x-a)}{(b-a)(c-a)}$ if $a \leq x < c$, $\frac{2(b-x)}{(b-a)(b-c)}$ if $c < x \leq b$	$[a; b]$
Uniform	a, b	$\frac{1}{b-a}$	$[a; b]$
Weibull	a, b, c	$\frac{c}{b}\left(\frac{x-a}{b}\right)^{c-1} \exp\left(-\left(\frac{x-a}{b}\right)^c \right)$	$[a; +\infty)$
Lognormal	a, b, c	$\frac{1}{\sqrt{2\pi}c(x-a)} \exp\left(-\frac{1}{2}\left(\frac{\ln(x-a)-b}{c}\right)^2 \right)$	$[a; +\infty)$

Table 1 Distributions of the random physical variables taken for the flood and the NRPV models.

Appendix B: Figures

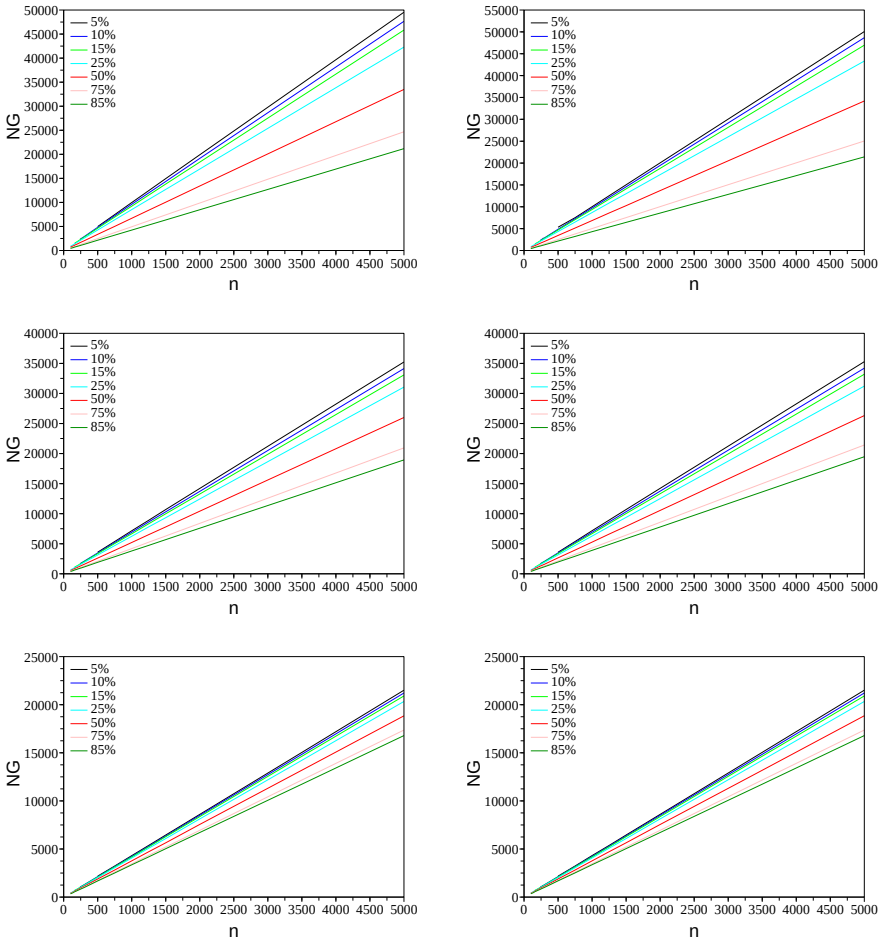

Fig. 1. Mean number of calls to the failure function depending on n and γ_1. $P_f = 10^{-4}$. $p = 3$. (Line 1) H_1. (Line 2) H_2. (Line 3) H_3. (Left) Non-recycling estimator. (Right) Recycling estimator.

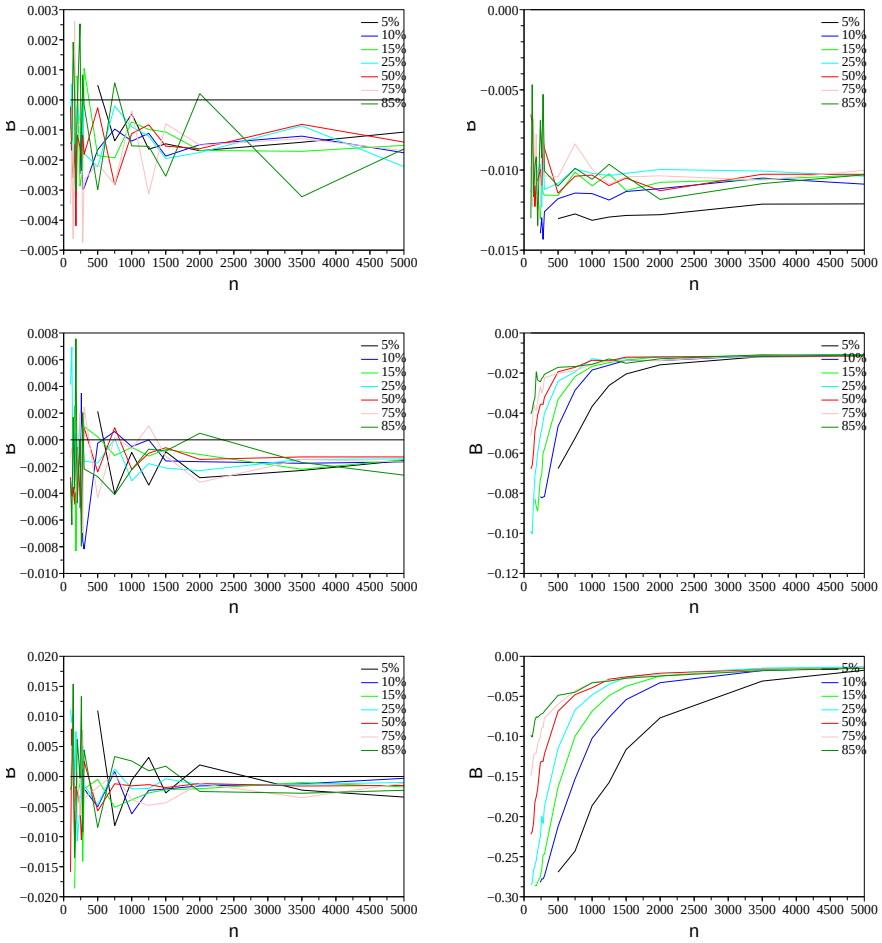

Fig. 2. Estimation of the relative bias depending on n and γ_1. $P_f = 10^{-4}$. $p = 3$. (Line 1) H_1. (Line 2) H_2. (Line 3) H_3. (Left) Non-recycling estimator. (Right) Recycling estimator.

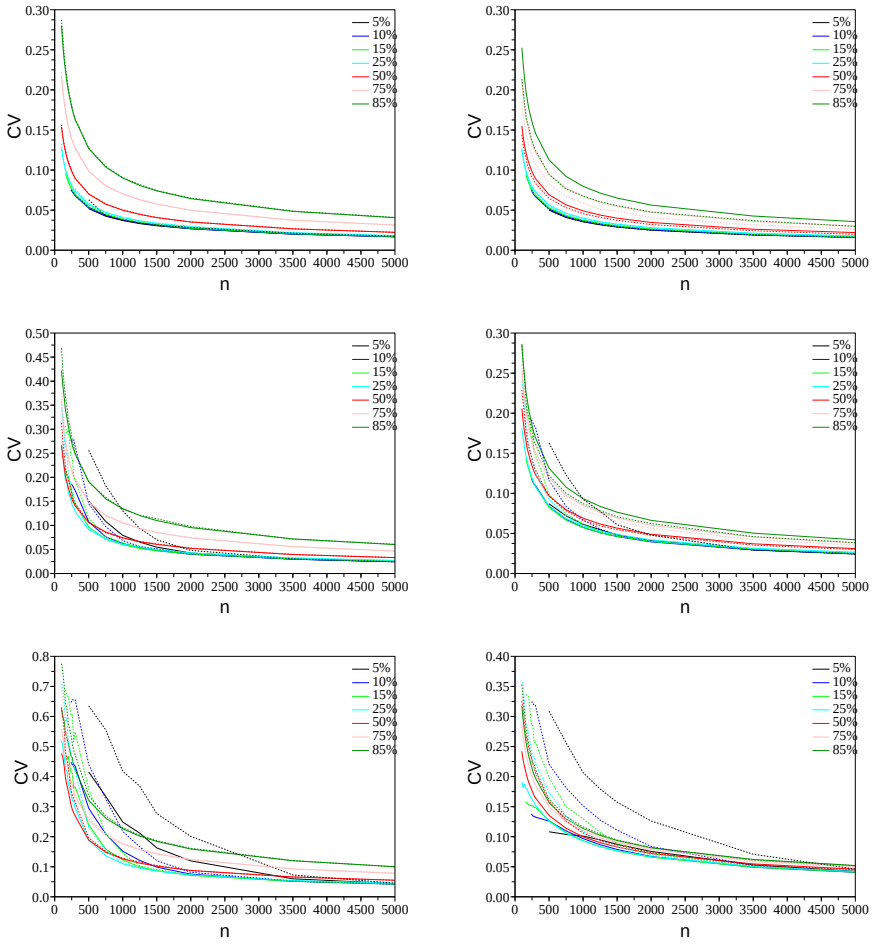

Fig. 3. Estimation of the coefficient of variation (full line) and the empirical coefficient of variation (dashed line) depending on n and γ_1. $P_f = 10^{-4}$. $p = 3$. (Line 1) H_1. (Line 2) H_2. (Line 3) H_3. (Left) Non-recycling estimator. (Right) Recycling estimator.

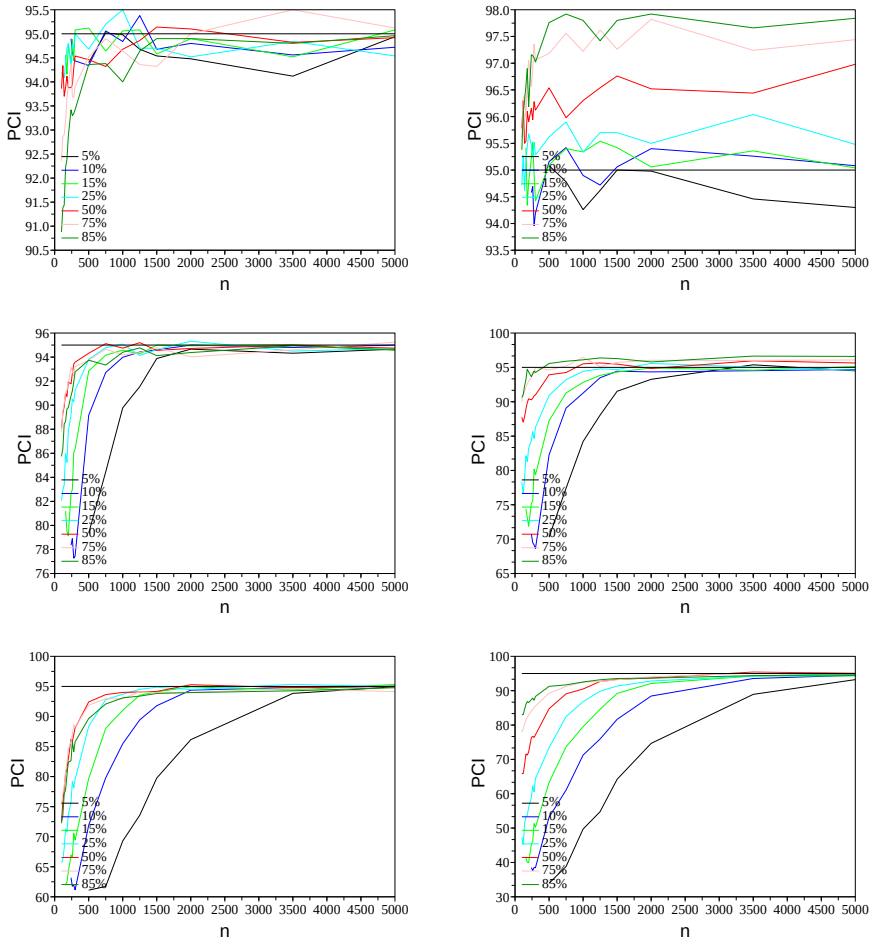

Fig. 4. Estimation of the percentage of estimations fallen in the estimated two-sided symmetric 95% confidence interval depending n and γ_1. $P_f = 10^{-4}$. $p = 3$. (Line 1) H_1. (Line 2) H_2. (Line 3) H_3. (Left) Non-recycling estimator. (Right) Recycling estimator.

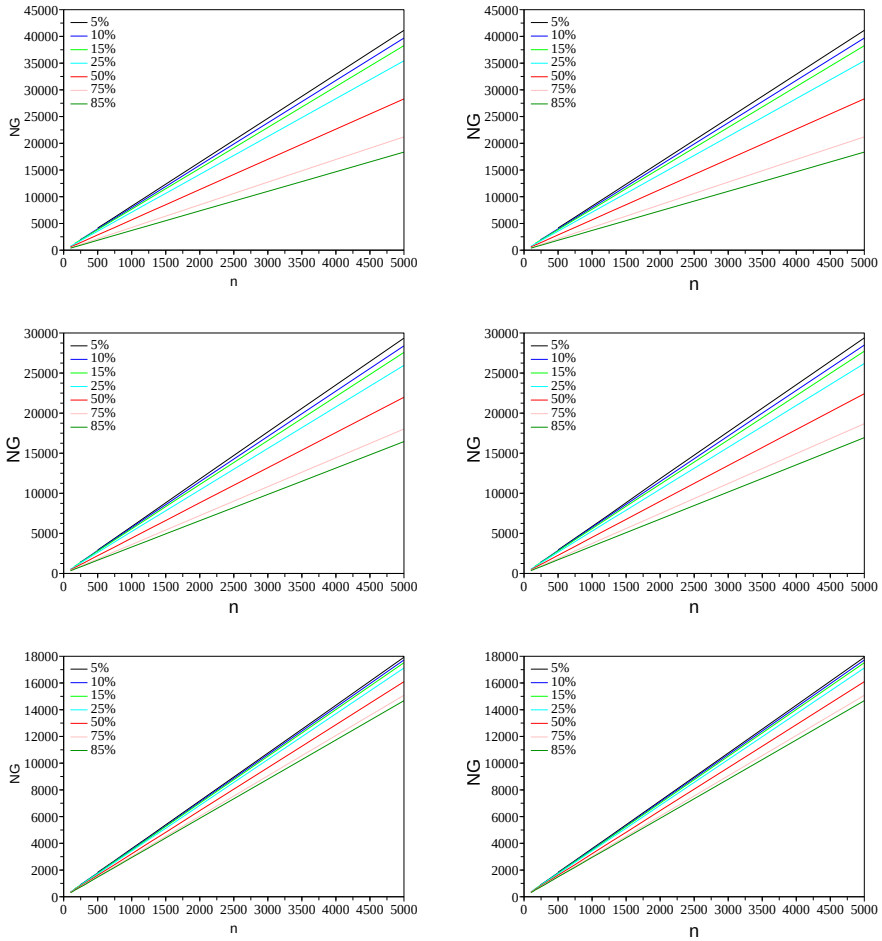

Fig. 5. Mean number of calls to the failure function depending on n and γ_1. $P_f = 10^{-8}$. $p = 3$. (Line 1) H_1. (Line 2) H_2. (Line 3) H_3. (Left) Non-recycling estimator. (Right) Recycling estimator.

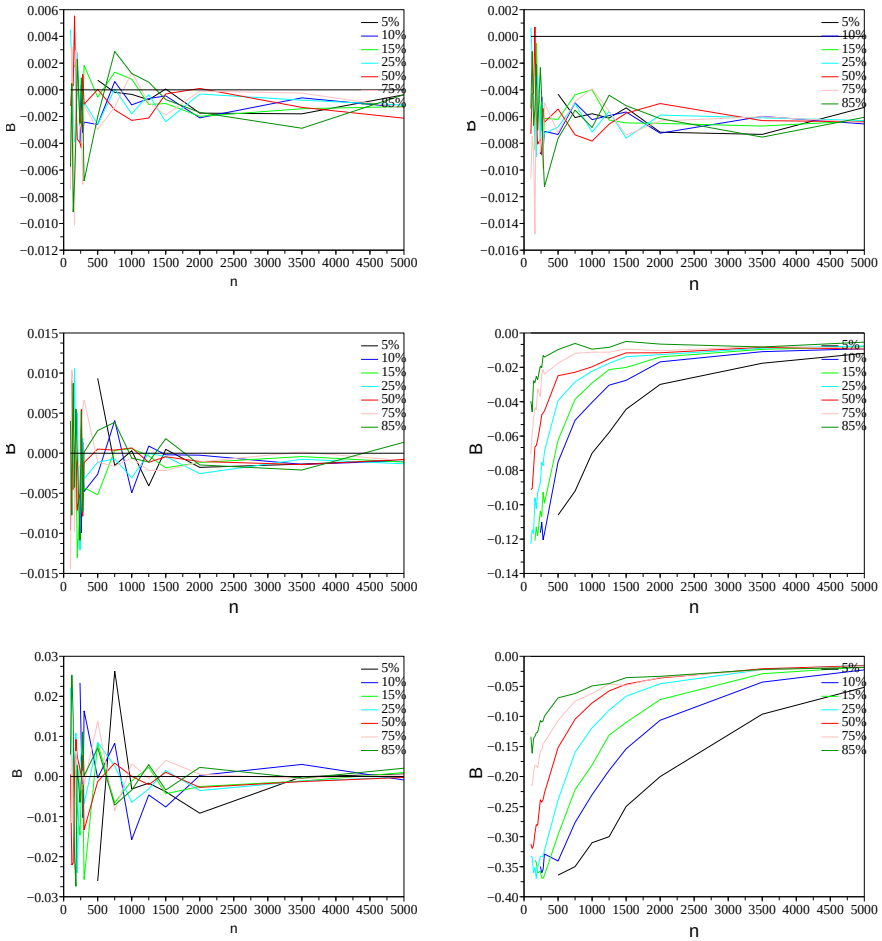

Fig. 6. Estimation of the relative bias depending on n and γ_1. $P_f = 10^{-8}$. $p = 3$. (Line 1) H_1. (Line 2) H_2. (Line 3) H_3. (Left) Non-recycling estimator. (Right) Recycling estimator.

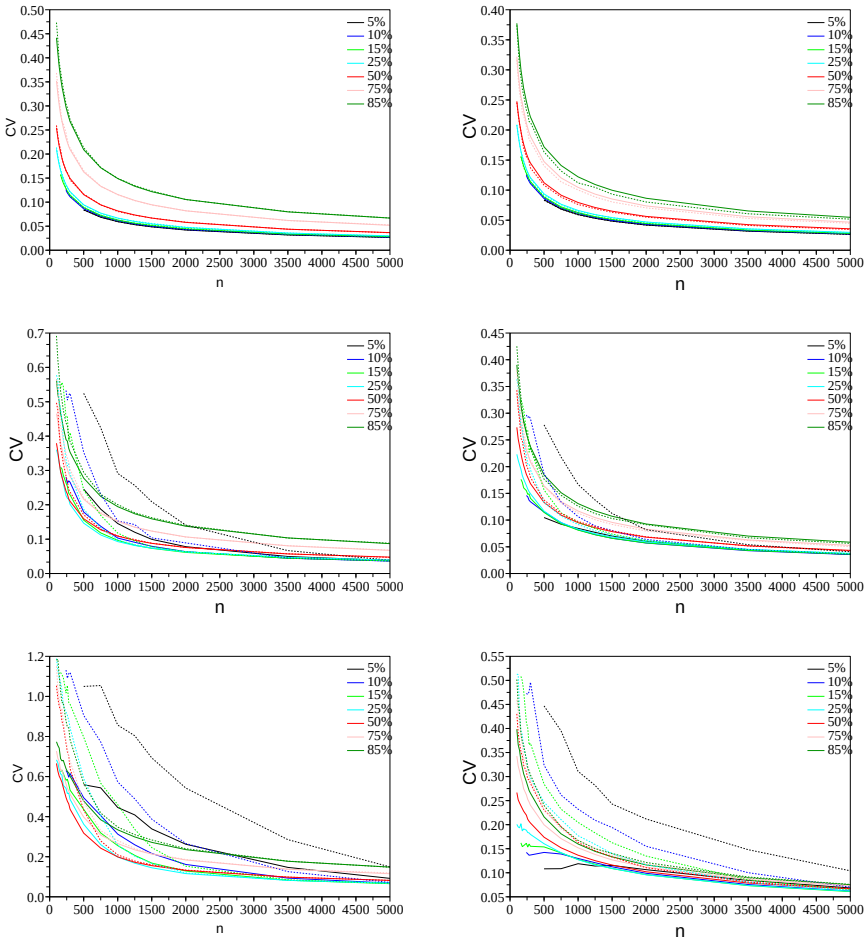

Fig. 7. Estimation of the coefficient of variation (full line) and the empirical coefficient of variation (dashed line) depending on n and γ_1. $P_f = 10^{-8}$. $p = 3$. (Line 1) H_1. (Line 2) H_2. (Line 3) H_3. (Left) Non-recycling estimator. (Right) Recycling estimator.

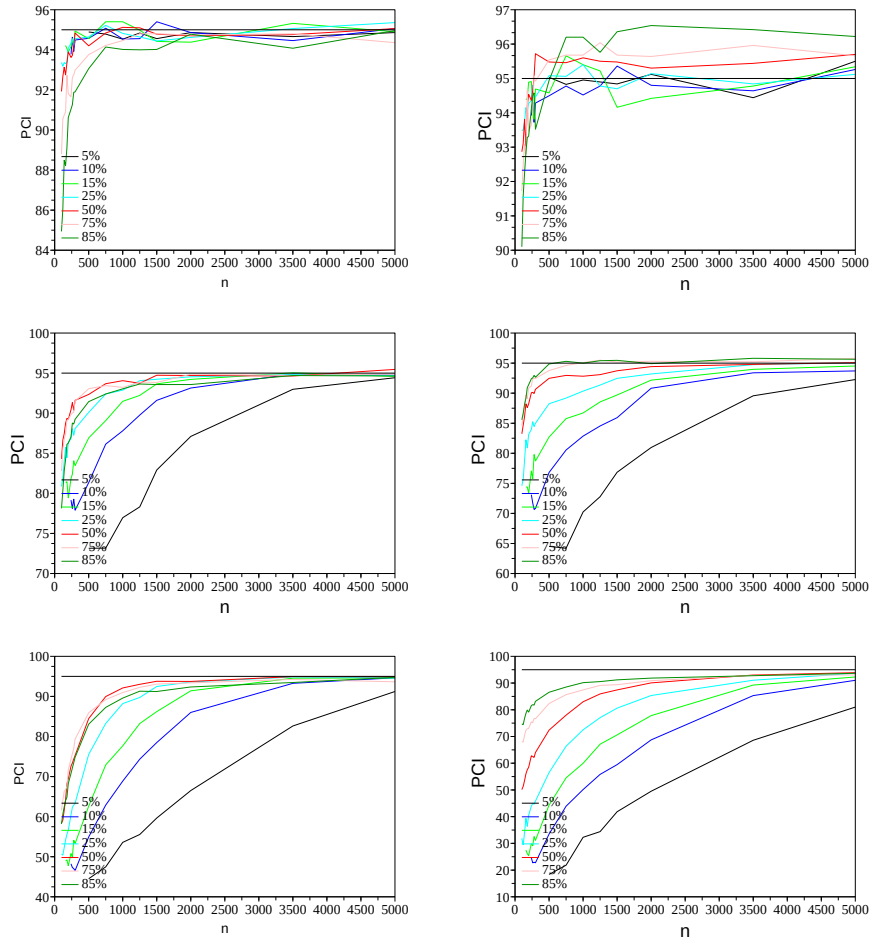

Fig. 8. Estimation of the percentage of estimations fallen in the estimated 95% confidence interval depending on n and γ_1. $P_f = 10^{-8}$. $p = 3$. (Line 1) H_1. (Line 2) H_2. (Line 3) H_3. (Left) Non-recycling estimator. (Right) Recycling estimator.

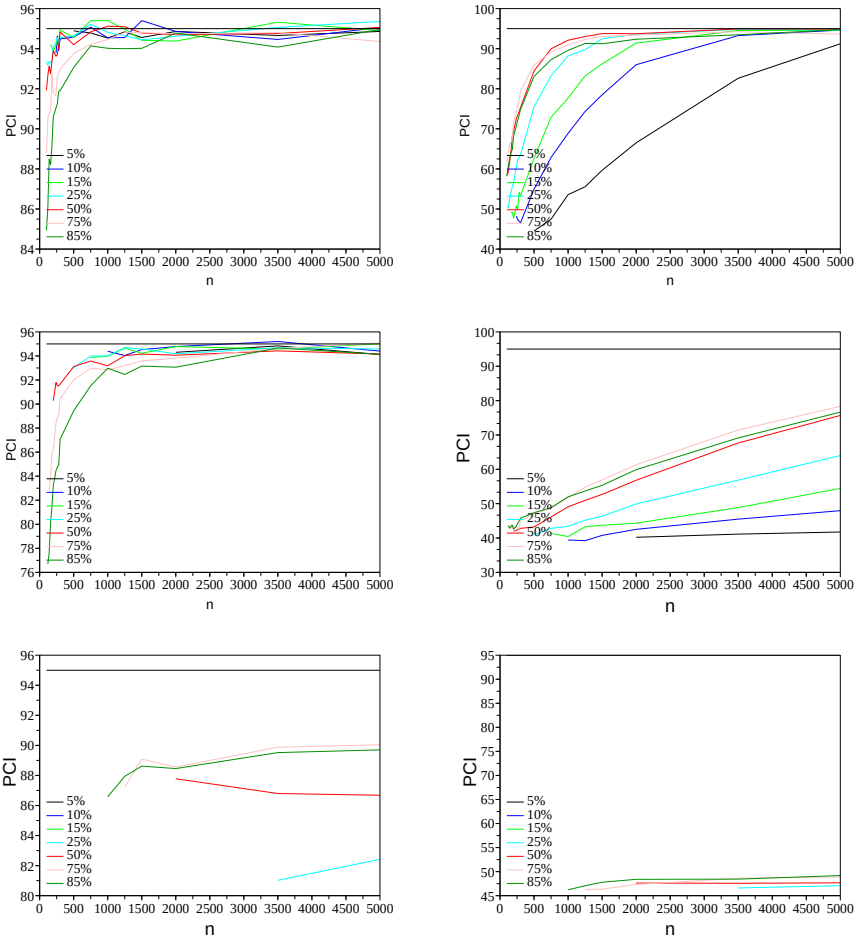

Fig. 9. Non-recycling estimator. Estimation of the percentage of estimations fallen in the estimated two-sided symmetric 95% confidence interval depending on n and γ_1. $P_f = 10^{-8}$. (Line 1) $p = 3$. (Line 2) $p = 5$. (Line 3) $p = 8$. (Left) H_1. (Right) H_3.